

1   **Comments to the Author:**

2   Reviewer #1 asked about the most significant parameter for improving aerosol  
3   distributions (Specific Comment #1). You respond by computing diversity, which is a  
4   normalized standard deviation. However, I don't think this quite addresses the comment.  
5   For example, for sulphate, its gaseous chemical production was highlighted as having the  
6   highest diversity (77%) among the 4 models that include this process. However, the  
7   standard deviation in absolute units is 0.26 Tg/yr. Compared to, say, the std dev for SO<sub>4</sub>  
8   emissions (0.84 Tg/yr) or wet deposition (1.21 Tg/yr), it's clear that even if gas phase SO<sub>4</sub>  
9   production was perfectly represented, its effect on SO<sub>4</sub> concentrations is not substantial  
10   enough to matter very much. Thus, diversity is not a very good metric for what models must  
11   improve to more accurately represent aerosol. I suggest that you use metrics that directly  
12   addresses the question.

13  
14   <Response>: The function of Table 3 is to quantify the diversity of these models over South Asia  
15   instead to reveal the discrepancies of models from observations. In order to answer the question  
16   of "the most significant parameter for improving aerosol distribution", we have to resort to  
17   detailed model sensitivity studies involving more model parameters. However, the multi-models  
18   in AeroCom portal do not provide this information. Therefore, in this study we only focus on  
19   identifying the possible causes of model underestimation of aerosol over South Asia. Despite large  
20   diversities among them, however, all models commonly underestimate AOD, indicating that some  
21   common model deficiencies exist. In Section 6, we suggested the most significant parameters  
22   associated with the underestimation of existing emissions sources (e.g. biofuel and agriculture  
23   waste) and missing aerosol species nitrate base on the comparison with the limited observations.  
24   As mentioned in our earlier response (and included in the previously revised version), in order to  
25   rank the relative contributions quantitatively, we will use one model (GEOSS) to conduct the  
26   sensitivity studies in a future study. The above information is mentioned in the conclusion part  
27   | (Page 23 of the marked-up manuscript).

28  
29   **To this end, Table 3 seems to show that SO<sub>4</sub> and dust are the main contributors to AOD, so**  
30   **whatever model parameters that are important for determining the concentrations of**  
31   **these aerosol types and exhibit the largest inter-model variability seem to be the ones that**  
32   **should be identified as most critical. It does not appear that the representation of OA or BC**  
33   **will matter nearly as much because they contribute little to AOD.**

34  
35   <Response> Based on the Table 3, SO<sub>4</sub> and dust are the major contributors to AOD in the models.  
36   This result is only based on the models, and thus it does not necessarily mean that the  
37   contribution of OA is lesser in the observation. For instance, the simulated AOD from OA is only  
38   1/3 of that from SO<sub>4</sub> averaged over South Asia (Table 3). However, OA likely contributes more to  
39   the total observed AOD than SO<sub>4</sub> does, indicated by its larger (exceeding twice) observed surface  
40   concentration at stations along IGP as shown in the following section. Unfortunately, we cannot  
41   quantify the relative contribution of individual aerosol species to total AOD in observations  
42   because we have limited ability to separate the individual AOD from the total. We added this  
43   comment in page 17 of the marked-up manuscript.

44  
45   **Response to Reviewer #1, Specific Comment #3: These are rather large discrepancies in the**  
46   **imaginary components of the various aerosol components. What are the consequences for**

47 modeled AOD, and hence for the model-obs comparisons of AOD? It seems like some  
48 discussion of this is warranted in the text.

49  
50 <Response> As shown in Table S1, we conducted Mie calculations for BC at 550 nm in CASE1 and  
51 CASE2, in which the refractive indices represent those used by the multi-models in this study.  
52 Moreover, in CASE3 and CASE4, we also consider additional scenarios with different real or  
53 imaginary parts to test the sensitivity of mass extinction efficiency (MEE) and single scattering  
54 albedo (SSA). As expected, the MEE and mass absorption efficiency (MAE, equal to  $MEE \times (1-SSA)$ )  
55 of BC are sensitive to changes of imaginary parts, because MAE dominates MEE. The MEE and MAE  
56 of BC are larger in the case with larger imaginary part. For example, from CASE1 to CASE3, given  
57 that the real parts are the same but the imaginary part is increased by 60% from 0.44 to 0.77, the  
58 MEE and MAE enhance by 40% and 47%, respectively. In addition, given that real parts are the  
59 same but the imaginary part increases by 11% from 0.71, that is used by three models in CASE 3,  
60 to 0.79 (recommended by Bond and Bergstrom (2006)) in CASE4, both the MEE and MAE enhance  
61 by 8%. On the other hand, the MEE of BC is less sensitive to the change of real part, but the MAE is  
62 sensitive. For example, from CASE3 to CASE2, given that imaginary parts are the same but the real  
63 part increase by 5% from 1.75 to 1.85, the MEE and MAE of BC reduces by 1% and 5%,  
64 respectively. In contrast, the mass scattering efficiency (MSE, equal to  $MEE \times SSA$ ) is the most  
65 sensitive to the increase of real part with MSE enhancing by 14%.

66 As for a more complicated situation in which both real and imaginary parts are different, the MEE  
67 and MAE enhance by ~40% from CASE 1 (representing the models HAD, GOC, SPR, GES) to CASE 2  
68 (representing the models ECH, GIE, GIM) with increasing both the imaginary and real parts.  
69 However, it is not necessary that the models in CASE 2 simulate higher AOD. For example, the  
70 model HAD shows higher AOD than the model ECH although the latter has higher real and  
71 imaginary parts (Fig. 4a and b). Therefore, this clearly suggests that there are other factors  
72 involved such as meteorology and emissions suppressing the simulated AOD by multi-models, as  
73 we have pointed out in the paper. Bond and Bergstrom (2006) attempted to increase BC  
74 imaginary part to 0.79, but this effort alone cannot remove the low bias of AAOD and AOD in  
75 models as suggested by this study. Bond et al. (2013) also pointed out that large differences in  
76 modeled horizontal and vertical transport are mostly responsible for the inter-model diversity of  
77 BC distributions.

78 Similarly, we conducted Mie calculation for dust in Table S2. The MEE of dust is dominated by  
79 scattering effect at the wavelength of 550nm. As expected, we found that the MEE and MAE of  
80 dust are insensitive to the change of imaginary part. For example, with the imaginary part  
81 increased by a factor of 7 from CASE 6 to CASE 7, the MEE and MAE of dust enhance by <1%. On  
82 the other hand, the MEE and MAE of dust are relatively sensitive to the change of real part. For  
83 example, with the real part increased by 2% from CASE 4 to CASE 5, both the MEE and MAE of  
84 dust enhance by 8%. The dust is minimal in the post-monsoon and the Winter period when the  
85 largest discrepancy occurs in models, however, small changes in values of imaginary and real  
86 parts of dust would not impact the AOD and AAOD simulations. Again, other factors such as  
87 meteorology and emissions are more likely dominant. We added the half of the above discussion  
88 to page 18 of the marked-up manuscript, and the remaining including Table S1 and S2 to the  
89 supplement.

94      **Table S1. The relationship of mass extinction efficiency (MEE) and single**  
 95      **scattering albedo (SSA) with refractive indices: BC.**

CASE <sup>1</sup>	Real <sup>2</sup>	Imaginary <sup>3</sup>	MEE <sup>4</sup>	SSA <sup>5</sup>	Note
1	1.75	0.44	5.4890E-16 m <sup>2</sup> /unit vol	0.2087	Used by HAD, GOC, SPR, GE5
2	1.85	0.71	7.5665E-16 m <sup>2</sup> /unit vol	0.1958	Used by ECH, GIE, GIM
3	1.75	0.71	7.6798E-16 m <sup>2</sup> /unit vol	0.1746	The same real part as CASE 1, the same imaginary as CASE 2
4	1.75	0.79 <sup>6</sup>	8.2873E-16 m <sup>2</sup> /unit vol	0.1723	The same real part as CASE 1, but with imaginary part recommended by Bond and Bergstrom (2006)

96      Note:

- 97      1. In all cases, modal radius = 0.0118  $\mu\text{m}$ , effective radius = 0.039  $\mu\text{m}$ , sigma =  
 98      2.0  $\mu\text{m}$ , density = 1.0 g/cm<sup>3</sup>, wavelength = 550 nm.  
 99      2. The real part of refractive index.  
 100     3. The imaginary part of refractive index.  
 101     4. Mass Extinction Efficiency, proportional to the aerosol optical depth (AOD).  
 102     5. Single scattering albedo. The Mass Absorption Efficiency (MAE) = MEE \* (1 -  
 103       SSA) and Mass Scattering Efficiency (MSE) = MEE \* SSA.  
 104     6. This value is recommended by Bond and Bergstrom (2006).

107  
108  
109  
110

Table S2. The relationship of mass extinction efficiency (MEE) and single scattering albedo (SSA) with refractive indices: dust.

CASE <sup>1</sup>	Real <sup>2</sup>	Imaginary <sup>3</sup>	MEE <sup>4</sup>	SSA <sup>5</sup>	Note
1	1.52	0.0015	1.5991E-14 m <sup>2</sup> /unit vol	0.9908	Used by HAD
2	1.53	0.0055	1.6432E-14 m <sup>2</sup> /unit vol	0.9675	Used by GOC
3	1.517	0.0011	1.5869E-14 m <sup>2</sup> /unit vol	0.9932	Used by ECH
4	1.564	0.002	1.7659E-14 m <sup>2</sup> /unit vol	0.9884	Used by GIE and GIM
5	1.53	0.002	1.6381E-14 m <sup>2</sup> /unit vol	0.9879	Used by SPR
6	1.53	0.008	1.6469E-14 m <sup>2</sup> /unit vol	0.9535	Used by GE5
7	1.53	0.0011	1.6368E-14 m <sup>2</sup> /unit vol	0.9933	The same real part as CASE 2, the same imaginary as CASE 3

111  
112 Note:  
113     1. In all case, modal radius = 0.042  $\mu\text{m}$ , effective radius = 1.4  $\mu\text{m}$ , sigma = 2.0  
114      $\mu\text{m}$ , density = 2.6 g/cm<sup>3</sup>, wavelength = 550 nm.  
115     2. The real part of refractive index.  
116     3. The imaginary part of refractive index.  
117     4. Mass Extinction Efficiency, proportional to the aerosol optical depth (AOD).  
118     5. Single scattering albedo. The Mass Absorption Efficiency (MAE) = MEE \* (1 -  
119       SSA) and Mass Scattering Efficiency (MSE) = MEE \* SSA.  
120  
121

122 |

123     **A multi-model evaluation of aerosols over South Asia:**

124         **Common problems and possible causes**

125     Xiaohua Pan<sup>1</sup>, Mian Chin<sup>1</sup>, Ritesh Gautam<sup>2</sup>, Huisheng Bian<sup>1,3</sup>, Dongchul Kim<sup>1,4</sup>, Peter R. Colarco<sup>1</sup>,  
126     Thomas L. Diehl<sup>1,4,\*</sup>, Toshihiko Takemura<sup>5</sup>, Luca Pozzoli<sup>6</sup>, Kostas Tsigaridis<sup>7,8</sup>, Susanne Bauer<sup>7,8</sup>,  
127             Nicolas Bellouin<sup>9</sup>

128     1. NASA Goddard Space Flight Center, Greenbelt, MD, United States.

129     2. Indian Institute of Technology, Bombay, Mumbai, India.

130     3. University of Maryland Baltimore City, Baltimore, MD, United States.

131     4. Universities Space Research Association, Columbia, MD, United States

132     5. Kyushu University, Fukuoka, Japan.

133     6. Istanbul Technical University, Istanbul, Turkey.

134     7. NASA, Goddard Institute for Space Studies, New York, NY, United States.

135     8. Center for Climate Systems Research, Columbia University, New York, NY, United States.

136     9. Department of Meteorology, University of Reading, Reading, Berkshire, United Kingdom.

137     \* Current address: European Commission at the Joint Research Center, Ispra, Italy

138

139     Correspondence to Xiaohua Pan (xiaohua.pan@nasa.gov)

140

141     **Abstract**

142     Atmospheric pollution over South Asia attracts special attention due to its effects on regional  
143     climate, water cycle and human health. These effects are potentially growing owing to rising  
144     trends of anthropogenic aerosol emissions. In this study, the spatio-temporal aerosol  
145     distributions over South Asia from seven global aerosol models are evaluated against aerosol  
146     retrievals from NASA satellite sensors and ground-based measurements for the period of  
147     2000-2007. Overall, substantial underestimations of aerosol loading over South Asia are found  
148     systematically in most model simulations. Averaged over the entire South Asia, the annual  
149     mean aerosol optical depth (AOD) is underestimated by a range 15% to 44% across models  
150     compared to MISR, which is the lowest bound among various satellite AOD retrievals (from  
151     MISR, SeaWiFS, MODIS Aqua and Terra). In particular during the post-monsoon and  
152     wintertime periods (i.e. October-January), when agricultural waste burning and anthropogenic  
153     emissions dominate, models fail to capture AOD and aerosol absorption optical depth (AAOD)  
154     over the Indo-Gangetic Plain (IGP) compared to ground-based AERONET sunphotometer  
155     measurements. The underestimations of aerosol loading in models generally occur in the lower  
156     troposphere (below 2km) based on the comparisons of aerosol extinction profiles calculated by  
157     the models with those from CALIOP data. Furthermore, surface concentrations of all aerosol  
158     components (sulfate, nitrate, organic aerosol and black carbon) from the models are found  
159     much lower than in-situ measurements in winter. Several possible causes for these common  
160     problems of underestimating aerosols in models during the post-monsoon and wintertime  
161     periods are identified: the aerosol hygroscopic growth and formation of secondary inorganic  
162     aerosol are suppressed in the models because relative humidity is biased far too low in  
163     boundary layer, the nitrate aerosol is either missing or inadequately accounted for, and  
164     emissions from agricultural waste burning and biofuel usage are too low in the emission

165 inventories. These common problems and possible causes found in multiple models point out  
166 directions for future model improvements in this important region.

167

## 168 1. Introduction

169 South Asia, particularly the Indo-Gangetic Plain (IGP) bounded by the towering Himalaya that  
170 is conducive to trapping both anthropogenic and dust aerosols (Fig. 1), is one of the global  
171 hotspots with persistent high aerosol optical depth (AOD) routinely observed by satellite  
172 remote sensors (e.g. Moderate Resolution Imaging Spectroradiometer or MODIS, Multi-angle  
173 Imaging SpectroRadiometer or MISR and Sea-Viewing Wide Field-of-View Sensor or  
174 SeaWiFS), as well as from ground-based measurements (e.g. Aerosol Robotic Network or  
175 AERONET). The potential influence of aerosols on the climate and water cycle in this region  
176 (e.g. Indian summer monsoon) via surface dimming and atmospheric warming has been widely  
177 discussed in the literature (e.g. Ramanathan et al., 2005; Lau et al., 2006). The atmospheric  
178 heating due to absorbing aerosols (mainly from black carbon i.e. BC) is estimated to be large  
179 especially in the wintertime, about  $50\text{--}70 \text{ W m}^{-2}$  (Ganguly et al., 2006). Recent studies have  
180 shown that the depositions of absorbing aerosols such as BC and dust over Himalaya are  
181 linked to snow albedo reduction and accelerated snow/ice melt in Himalaya during the pre-  
182 monsoon season (Lau et al., 2010; Qian et al., 2011; Yasunari et al., 2010; Gautam et al.,  
183 2013).

184 Besides these climate impacts, fine aerosol particles ( $\text{PM}_{2.5}$ ) are known to affect public  
185 health, especially over IGP where large portions of the Indian population live. At Delhi, for  
186 example,  $\text{PM}_{2.5}$  concentration in 2007 was  $97\pm56 \mu\text{g/m}^3$  (Tiwari et al., 2009), nine times the air  
187 quality guidelines recommended by the World Health Organization in 2005. Increases in  
188 anthropogenic aerosol emissions and loading in South Asia in recent decades have been well  
189 documented (Ohara et al., 2007; Hsu et al., 2012; Kaskaoutis et al., 2012; Babu et al., 2013),  
190 in contrast with the decreasing emission trends over Europe and North America (Granier et al.,  
191 2011; Diehl et al., 2012). Therefore, it is critical to accurately represent aerosol sources,  
192 distributions and properties in models over this heavily polluted region in order to project the  
193 future climate and air quality changes in South Asia with confidence.

194 Previous studies, however, reported that global models generally underestimated  
195 aerosol loading over South Asia, especially over the IGP in winter (Reddy et al., 2004; Chin et  
196 al., 2009; Ganguly et al., 2009; Henriksson et al., 2011; Goto et al., 2011; Cherian et al., 2013;  
197 Sanap et al., 2014). Among them, Ganguly et al. (2009) reported that the GFDL-AM2 model  
198 largely underestimated the AOD over the IGP during winter by a factor of 6. Recently, AOD  
199 simulated by the regional climate model (RegCM4) showed higher correlation with AERONET  
200 AOD at stations over dust-dominated areas in south Asia than over the regions dominated by  
201 anthropogenic aerosols, i.e. 0.71 vs. 0.47 (Nair et al., 2012). Eleven out of twelve models  
202 participating in the Aerosol Comparisons between Observations and Models (AeroCom) phase  
203 I exercise were also found to underestimate the aerosol extinction over South Asia, especially  
204 under 2 km, in comparison with the space-borne lidar measurements from the Cloud-Aerosol  
205 Lidar and Infrared Pathfinder Satellite Observations (CALIPSO) satellite (Koffi et al., 2012).

206 The ability to capture surface BC concentrations over South Asia for models has also been  
207 found to be limited, with the low biases that tend to be larger in winter (Ganguly et al., 2009;  
208 Menon et al., 2010; Nair et al., 2012; Moorthy et al., 2013). A very recent study evaluating the  
209 latest generations of quasi-operational aerosol models participating in International  
210 Cooperative for Aerosol Prediction (ICAP) has shown that the models have very low skill  
211 scores in reproducing AERONET measured AOD at Kanpur, an urban city in northern India  
212 (Sessions et al., 2015). These studies underscore great challenges for current global aerosol  
213 models to adequately represent aerosols in South Asia.

214 Extending from previous studies and utilizing the recent model outputs from the  
215 AeroCom Phase II multi-model experiments, the present work systematically evaluates aerosol  
216 simulations in South Asia by seven global aerosol models with observations from satellites and  
217 ground-based measurements, and strives to characterize the model deficiency in reproducing  
218 observations. The outcomes of this study will help us understand the discrepancies between  
219 models and observations, thus providing directions for future model improvements in this  
220 important region.

221 The description of models is given in Section 2, followed by the introduction of  
222 observational data from satellites and ground-based measurements in Section 3. The model  
223 results are compared with observations in Section 4, including the spatial and temporal  
224 distribution of AOD and aerosol absorption optical depth (AAOD), vertical profile of aerosol  
225 extinction coefficient, and the surface BC concentration. The diversity among models is  
226 discussed in Section 5, and possible causes for the model underestimations of aerosol  
227 amounts are investigated in Section 6. Major findings are summarized in Section 7.  
228

## 229 **2. Model description**

### 230 **2.1 Models**

231 Aerosol simulations for the period of 2000-2007 from seven models, including six models that  
232 participated in AeroCom Phase II hindcast experiment (i.e. AeroCom II HCA) and one  
233 additional model, GEOS5, are analyzed in this paper (see Table 1 for details). Note that the  
234 model outputs related to aerosol optical properties, such as AOD, AAOD and extinction  
235 coefficient, are at the wavelength of 550 nm. Given that MODIS and MISR are available only  
236 after 2000, we chose the years 2000-2007 in this study although longer time period of  
237 simulations (starting from 1980) are available from the AeroCom models (note that ECHAM5-  
238 HAMMOZ ended in 2005 and HadGEM2 in 2006). Aerosol modules in GEOS5 are based on  
239 GOCART with some modifications (Colarco et al., 2010). More detailed descriptions about  
240 these models can be found in previous studies (see references listed in Table 1 and Myhre et  
241 al., 2013). All models include sulfate ( $\text{SO}_4^{2-}$ ), BC, organic aerosol (OA), dust (DU) and sea salt  
242 (SS). Nitrate ( $\text{NO}_3^-$ ) is included only in three models (GISS-modelE, GISS-MATRIX and  
243 HadGEM2). The secondary organic aerosol (SOA) chemistry is resolved in two models, GISS-  
244 modelE and HadGEM2, whereas simple parameterizations of SOA are used in the remaining  
245 models. There are some differences among the seven models on aerosol optical properties  
246 (see refractive indices listed in Table 1). In comparison with satellite retrievals and AERONET  
247 observations that are available only under clear-sky conditions, it is desirable to use the

modeled AOD for clear-sky as well; however only two GISS models provide such output (other models just provide all-sky results). In general, clear-sky AOD is lower than all-sky AOD, for example, by 20% globally based on the GEOS-Chem model (Yu et al., 2012). All seven models use the assimilated wind fields although from different datasets. The horizontal resolutions vary from 2.8° by 2.8° (ECHAM5-HAMMOZ) to 1.1° by 1.1°(SPRINTARS) and the vertical levels range from 30 (GOCART-v4) to 72 (GEOS5) intervals. More information is given in Table 1.

## 2.2 Emissions

For anthropogenic emissions, which are mainly from consumption of fossil fuel and biofuel, the models use either A2-ACCMIP or A2-MAP emission dataset that are provided for the AeroCom Phase II model experiments (Diehl et al., 2012). Both A2-ACCMIP and A2-MAP were constructed by combining multiple inventories but in different ways. The annual anthropogenic emissions from A2-MAP are yearly emission dataset with inter-annual variability, while those from A2-ACCMIP are without actual inter-annual variability, simply generated by linear interpolation between decadal endpoints except for biomass burning (Granier et al., 2011; Diehl et al., 2012). Over South Asia, the spatial distribution and total emission amount are somewhat different between the two emission datasets, with higher emission amount in A2-ACCMIP. Detailed information on both emission datasets can be found in Diehl et al. (2012).

Figure 2 shows the averaged annual mean (2000-2007) anthropogenic BC, organic aerosol (OC), SO<sub>2</sub>, NH<sub>3</sub> and NO<sub>x</sub> emissions in South Asia from A2-ACCMIP anthropogenic emission dataset (A2-MAP is not shown and it does not provide NH<sub>3</sub> and NO<sub>x</sub> emissions). In this study, we define the South Asia domain as 60°E–95°E longitude and 5°N –36°N latitude. Note that the seasonal cycle of anthropogenic emission is not resolved in either emission datasets, which could be problematic especially for biofuel emission in this region (discussed in Section 6.3). The anthropogenic emissions display high spatial heterogeneities over South Asia, coinciding with the population density distribution as reported by previous studies (e.g. Girolamo et al., 2004). Densely populated regions are usually associated with heavy anthropogenic emissions in South Asia, especially over IGP. The annual mean anthropogenic aerosols emission in South Asia for the period of 2000-2007 from A2-ACCMIP (A2-MAP) are 7.46 (5.33) Tg yr<sup>-1</sup> of SO<sub>2</sub>, 5.94 Tg yr<sup>-1</sup> of NH<sub>3</sub>, 4.50 Tg yr<sup>-1</sup> of NO<sub>x</sub>, 2.18 (1.71) Tg C yr<sup>-1</sup> of OC, and 0.69 (0.65) Tg C yr<sup>-1</sup> of BC. The ratio of OC/BC anthropogenic emissions (fossil fuel and biofuel) is 3.2 (2.6) over South Asia.

Open biomass burning including the agricultural residue burned in the field and forest fires contributes to 25% of total BC (and OC) emissions over India based on the estimation by Venkataraman et al. (2006) with the difference between the total crop waste and that used as fuel and animal fodder. Figure 3 shows the seasonal BC biomass burning emission based on monthly Global Fire Emissions Database Version 2 (GFED2), which is used by both A2-ACCMIP and A2-MAP emission datasets. The open biomass burning displays strong spatial and seasonal variations. Pre-monsoon period is the most active open biomass burning season with an emission amount of 0.22 Tg C yr<sup>-1</sup> of BC over South Asia, concentrated over

289 northeastern India associated with the Jhum cultivation to clear the forest and create fields  
290 (Vadrevu et al., 2013). Seasonal practices of biomass burning of agricultural crop residues  
291 associated with rice-wheat crop rotation over the western IGP, such as Punjab, Haryana and  
292 western Uttar Pradesh, could explain the high aerosol loading during the post-monsoon of  
293 October-November (Badarinath et al., 2009a; Sharma et al., 2010; Vadrevu et al., 2011;  
294 Vadrevu et al., 2013) with a total emission amount of  $0.001 \text{ Tg C yr}^{-1}$  BC over South Asia in  
295 GFED2. The ratio of OC/BC open biomass burning emission is 8.0 averaged over South Asia.

296 The major natural aerosol over South Asia is the wind-blown mineral dust from the arid  
297 and semi-arid regions of southwest Asia, such as Iran, Afghanistan, Pakistan, Arabian  
298 Peninsula, and Thar Desert in the northwestern India. The dust emissions are calculated by  
299 each model and show a large diversity varying from  $10.6 \pm 3.3$  (ECH) to  $185.8 \pm 33.6$  (SPR)  $\text{Tg yr}^{-1}$   
300 over South Asia (averaged for 2000-2007). This model diversity is attributed to differences  
301 in the model size bins of dust aerosols, parameterization of source strength, and wind fields  
302 and soil properties over source regions (see more detailed discussions in Section 5). Sea salt  
303 emission is negligible for the study area.

### 304 3. Observational datasets

#### 305 3.1 Satellite data

306 In this study, five satellite products are used to characterize aerosol distribution and  
307 evaluate the model simulations. MODIS Terra and Aqua level-3 monthly mean AOD products  
308 at 550nm wavelength (Collection 5.1) are used by averaging the daily aerosol products at  
309  $1^\circ \times 1^\circ$  grid. The MODIS AOD is a composite of the Dark Target (Levy et al., 2007 and 2010)  
310 and Deep Blue retrieval products (Hsu et al., 2006), as the latter is able to retrieve AOD over  
311 bright surfaces such as the Thar Desert in South Asia. SeaWiFS level-3 monthly AOD  
312 products at 550nm (V003) are obtained by averaging the daily aerosol products at  $1^\circ \times 1^\circ$  grid.  
313 SeaWiFS retrieval adopts the Deep Blue algorithm over land (Hsu et al., 2006, 2012) and  
314 Ocean Aerosol Retrieval (SOAR) algorithm over ocean (Sayer et al., 2012 and 2013). MISR  
315 level-3 monthly AOD products at 555nm (V004) are used by averaging the weekly aerosol  
316 products at  $0.5^\circ \times 0.5^\circ$  grid. MISR retrieves aerosol properties over a variety of terrain including  
317 bright surface like deserts (Martonchik et al., 2004; Kahn et al., 2007 and 2010). In spite of the  
318 fact that the satellite data are instantaneous observations at local overpass times (varying  
319 between 10:30AM to 1:30PM for MODIS, MISR, and SeaWiFS) while models outputs are  
320 diurnally varying, any bias caused by diurnal vs. instantaneous sampling is expected to be  
321 small for monthly mean AOD. The study by Colarco et al. (2010) compared model simulated  
322 AOD sampled at MODIS/MISR overpass times with those averaged over diurnal time steps  
323 and found the differences to be small for monthly mean AOD, with only about 10% difference  
324 in south America and southern Africa (i.e. biomass burning regions) and smaller elsewhere.

325 The climatology (averaged over the period of June 2006-December 2011) of vertical  
326 extinction profiles from the Cloud-Aerosol Lidar with Orthogonal Polarization (CALIOP) layer  
327 product version 3.01(onboard CALIPSO satellite) is used to evaluate the model simulated  
328 aerosol vertical distribution in 2006 (CALIPSO 2011; Koffi et al., 2012). Only the CALIOP

330 observations in 532 nm channel for nighttime are used because of their better signal-to-noise  
331 compared to daytime observations. Three aerosol parameters are used to inter-compare  
332 model simulations with CALIOP, namely AOD,  $Z_a$  (km) and  $F_{2km}$  (%). AOD is the integral of  
333 extinction coefficient within the entire column (Eq.1).  $Z_a$  is defined as the averaged aerosol  
334 layer height (Eq. 2), and  $F_{2km}$  is defined as the percentage of AOD located in the lowest 2 km  
335 (Eq. 3) in the column.

336

$$AOD = \sum_{i=1}^n EXT_i \times \Delta Z_i \quad (1)$$

$$Z_a = \frac{\sum_{i=1}^n EXT_i \times Z_i}{\sum_{i=1}^n EXT_i} \quad (2)$$

$$F_{2km} = \frac{\sum_{i=1}^{level\ of\ 2km} EXT_i \times \Delta Z_i}{\sum_{i=1}^n EXT_i \times \Delta Z_i} \quad (3)$$

340

### 341 3.2 AERONET

342 In this study, we use AOD and AAOD data from the ground-based AERONET (Holben et al.,  
343 1998) sites in South Asia. Monthly mean AOD and AAOD were analyzed over Kanpur, Lahore  
344 and Karachi. Level-2 (version 2) data are used, which are cloud-screened and quality-assured  
345 aerosol products with a low uncertainty of 0.01–0.02. Locations of the three stations are shown  
346 in Fig.1 along with eleven in-situ measurement sites as described in the following Section 3.3.  
347 The information of all fourteen ground-based measurement sites is given in Table 2.

348

### 349 3.3 In-situ measurements

350 Modeled BC concentrations are also evaluated with the surface in-situ measurements from the  
351 Integrated Campaign for Aerosols gases and Radiation Budget (ICARB) field campaign in  
352 India over eight stations, which spread over Indian mainland and islands for the entire year of  
353 2006. The BC data from ICARB field campaign were measured by inter-compared  
354 aethalometers following a common protocol. More details of ICARB measurements can be  
355 found in previous publications (e.g. Beegum et al., 2009 and Moorthy et al., 2013).

356 In order to examine the aerosol chemical composition (such as surface concentrations  
357 of nitrate, sulfate, organic aerosol and black carbon) and meteorological conditions (such as  
358 surface relative humidity and temperature) of winter haze over IGP in multi-models, we refer to  
359 measurements from the Indian Space Research Organization- Geosphere Biosphere  
360 Programme (ISRO-GBP) campaign which provided valuable information about aerosol  
361 physical, optical and chemical properties along the IGP during the wintertime of December  
362 2004. For this study, four stations in IGP are selected because of their relatively complete  
363 measurements. They are Hisar (Ramachandran et al., 2006; Rengarajan et al., 2007; Das et  
364 al., 2008), Agra (Safai et al., 2008), Kanpur (Tripathi et al., 2006; Tare et al., 2006) and  
365 Allahabad (Ram et al., 2012a), from western to eastern IGP. Note that the in-situ data used in  
366 this study are obtained from the aforementioned references.

367

### 368 4. Results

369 In this section, the aerosol simulations by multi-models are evaluated in comparison to satellite  
370 data and ground-based measurements in terms of temporal variation and spatial distribution  
371 (horizontally and vertically) over South Asia.

372

#### 373 **4.1 Interannual variability of AOD**

374 Figure 4a shows the annual averaged mean AOD over the entire South Asia domain (land only,  
375 shown in gray shaded area) for the period of 2000-2007. AODs are  $0.270 \pm 0.008$  and  
376  $0.273 \pm 0.012$  from MISR and SeaWiFS (SeaW) retrievals respectively, and  $0.326 \pm 0.010$  and  
377  $0.332 \pm 0.018$  from MODIS Aqua (MODIS-a) and Terra (MODIS-t) respectively. MISR AOD is  
378 the lowest bound of four satellite retrievals. The difference in AODs among satellite data is  
379 significant and could be up to 0.062 or 22% of MISR. Six out of seven models (except for  
380 HAD) consistently underestimated AOD by 0.043-0.119 or 15%-44% relative to MISR. As  
381 shown in Fig. 4b, over the central IGP region ( $77\text{-}83^\circ\text{E}/25\text{-}28^\circ\text{N}$ , denoted by the red box in Fig.  
382 4a) where the hotspot of AOD is observed from satellites, the performance of the same six  
383 models are even worse, with the annual averaged mean AOD underestimated by 20-57%  
384 relative to MISR. Unlike other models, HAD shows comparable AOD with MISR and SeaWiFS  
385 over the entire South Asia (Fig.4a), but exceeds all satellite data over the central IGP (Fig.4b),  
386 higher than SeaWiFS and MISR by 47% and 58% respectively, and higher than MODIS-Terra  
387 and Aqua by 16% and 20% respectively. As shown in Figure 4a, the peak AOD in 2003 and  
388 the low AOD in 2005 appear in all satellite data (except MODIS Aqua in 2003), which are  
389 associated with the strength of dust emissions during the dry season in the same years  
390 (Kaskaoutis et al., 2012; Hsu et al., 2012; Ramachandran et al., 2013). However, all models  
391 fail to reproduce the peak AOD in 2003, whereas only two models (GE5 and SPR) indicate the  
392 low AOD in 2005.

393

#### 394

#### 395 **4.2 Seasonal cycle of AOD and AAOD over 3 AERONET stations**

396 To further examine the details of underestimations occurring in most models, we compare the  
397 model-simulated monthly variations of AOD and AAOD with the AERONET data at three  
398 selected sites in South Asia (Fig. 5). These locations represent different aerosol environments  
399 in South Asia: Kanpur, an industrial city located in the central IGP, is influenced by high  
400 anthropogenic emissions throughout the year and by the transported dust during pre-monsoon  
401 (MAM) and early monsoon periods (JJ); Lahore, an urban city located in the western IGP, is  
402 directly influenced by biomass burning in the pre-monsoon (MAM) and post-monsoon (ON)  
403 seasons; and Karachi, an urban coastal city in Pakistan, is influenced by frequent dust  
404 outbreaks, especially from the Arabian peninsula around early summer monsoon season (JJ).  
405 A two-year period is chosen for each site based on the availability of AERONET  
406 measurements. Three satellite datasets, namely MODIS-Aqua, MISR, and SeaWiFS, are also  
407 displayed to draw inter-comparison of AOD with AERONET data.

408 At Kanpur (first row of Fig. 5), strong seasonal variation of AERONET AOD (left column  
409 in Fig. 5) is evident with two peaks, one in May-July associated with dust outbreaks and the  
410 other in October-January associated with active open biomass burning as well as high

anthropogenic emissions. However, most models (except for HAD) only show the peak in May-July but miss the peak in October-January. Although the HAD model simulates two seasonal maxima, they disagree with the peak months observed from AERONET. Overall, AOD from all models have weak or negative correlation coefficients with AERONET data (from -0.34 to 0.34), with four models anti-correlated with AERONET data (ECH, GIM, GOC and HAD), and one with no correlation (GIE). AODs from six models are lower than those from AERONET as indicated by the relative biases ranging from 0.31 to 0.74. In contrast, HAD model overestimate the AOD by 44% (relative bias of 1.44). As for AAOD (right column in Fig. 5), models are much lower than the AERONET data by a factor of 2 on average, suggesting the underestimation of BC loading or weak aerosol absorption strength in models (see more analysis of BC in Section 4.5).

At Lahore (second row of Fig. 5), AERONET data are mostly available in the year 2007, when only five model results are available (no HAD and ECH for 2007, see Table 1). Lahore is located in the Punjab region, which is an agriculture region known as the “breadbasket” for Pakistan and India. The enhanced AERONET AOD and AAOD are evident at Lahore during October-November, which is linked to the agricultural waste burning after harvest. However, all five models largely underestimate AOD and AAOD in the October-November period. This suggests that emissions from agriculture waste burning are likely underestimated in GFED2 that are used by the models (discussed in Section 6.4). Compared to observations, HAD again showed abnormal seasonal variation at Lahore, similar to that at Kanpur, with extreme high AOD in October though.

At Karachi (third row of Fig. 5), a unimodal seasonal distribution is revealed in AERONET AOD data, in contrast to the bimodal seasonal variation at Kanpur. The maximum AOD around July is associated with the wind-driven mineral dust from the Arabian Peninsula, which is captured by the models as indicated by relatively strong correlation from 0.58 to 0.91 (except HAD. Note ECH is not available for 2006-2007). However, similar to other sites, AOD from all models are too low in late autumn to winter. Models also fail to capture the relatively higher AAOD around November that is associated with smoke transported from agriculture waste burning in northwestern IGP (i.e. the area around Lahore) (Badarinath et al., 2009a,b).

Overall, in comparison with AERONET at three sites, most models tend to significantly underestimate AOD in October-January when aerosols from agriculture waste burning and anthropogenic activities are dominant. On the other hand, the monthly variations and magnitudes of AOD from the satellites are in general similar to those from AERONET. As an exception, MODIS-Terra<sup>1</sup> is biased high (up to a factor of 2) during pre-monsoon and monsoon months. This overestimation of AOD partially results from low bias of surface reflectance under dusty conditions in the MODIS Dark-Target aerosol retrieval algorithm (Jethva et al., 2009).

In order to diagnose the discrepancies between models and AERONET data, the individual component AOD from four models (HAD, GE5, SPR and GOC, unavailable from other three models) are examined at Kanpur for 2004 in Fig. 6. We choose the year of 2004 because ISRO-GBP campaign took place in the same year (see Section 3.3 and Section 6), so that we can intercompare AERONET data with that in ISRO-GBP campaign. In December and

Xiaohua 4/15/2015 2:26 PM

Deleted: Aqua

453 January, AOD from AERONET data is around 0.7, dominated by anthropogenic contributions  
454 (about 75%, estimated by Tripathi et al. 2006). All four models have difficulties to capture the  
455 magnitude of AOD in December and January. Among them, AOD from HAD (upper left panel  
456 in Fig. 6) matches relatively well with AERONET data, capturing about half of the observed  
457 value. Interestingly, nitrate ( $\text{NO}_3^-$ ) AOD is the major component in HAD, contributing to 50% of  
458 total modeled AOD. In contrast, three other models (SPR, GE5 and GOC) largely  
459 underestimate the peak in the winter (December and January) by up to a factor of 7. As a  
460 common problem, these three models do not include the nitrate aerosol component. During the  
461 months of May to July, coarse mode aerosol (i.e. dust) contributes mostly to total AOD (> 60%)  
462 based on studies with ground based sun/sky radiometer data (e.g. Srivastava et al., 2012a).  
463 SPR and GE5 capture this feature while HAD and GOC underestimate the contribution of dust.  
464 In the HAD model, AODs from nitrate alone during April and October are comparable to  
465 column total AERONET AOD, indicating a problem in representing seasonal variation of nitrate  
466 in HAD, as shown in Fig. 5. Instead, nitrate aerosol is expected to peak in winter because of  
467 high relative humidity and low temperature over IGP that favor the formation of  $\text{NH}_4\text{NO}_3$  (Feng  
468 and Penner 2007; Ram et al., 2010b; Ram et al., 2012b).

469 Overall, Fig. 6 demonstrates that the magnitudes and seasonal cycles of aerosol  
470 compositions are quite different across the models. Further examination of the model  
471 diversities will be discussed in Section 5.

#### 473 **4.3 Spatial distribution of AOD in different seasons**

474 In this section, we compare the spatial distributions of AOD over the entire South Asia and  
475 neighboring oceans among four satellite products (MODIS-Terra, MODIS-Aqua, MISR, and  
476 SeaWiFS) and seven model simulations during the winter monsoon (DJF), pre-monsoon  
477 (MAM), summer monsoon (JJAS) and post monsoon (ON) phases averaged over 2000-2007,  
478 shown in Fig. 7a-b. Locations of the three aforementioned AERONET stations are also labeled  
479 in the maps for reference. In general, the spatial distribution of AOD is closely associated with  
480 the emission source over South Asia, and the aerosol abundance in the atmosphere is  
481 modulated by meteorological conditions, such as efficient atmospheric dispersion associated  
482 with the strengthened westerly flow in March-July, high wet removal associated with the  
483 monsoon rainfall in June–September, and stable atmospheric conditions and thus less efficient  
484 atmospheric dispersion in December-February.

485 During the winter season (DJF), local anthropogenic sources dominate over dust,  
486 contributing as much as 80% ( $\pm 10\%$ ) to the aerosol loading (Ramanathan et al., 2001; Tripathi  
487 et al., 2006). The maximum AOD is found in the central and eastern IGP based on four  
488 satellite datasets as shown in Fig. 7a, which coincides with clusters of coal-based large  
489 thermal power plants (capacity >1970 MW) (Prasad et al., 2006). The natural topography (i.e.  
490 gradually decreased elevation eastward but narrow opening to the Bay of Bengal as shown in  
491 Fig. 1) is conducive to the accumulation of aerosol over central and eastern IGP. Additionally,  
492 the winter season is characterized by relatively stable atmospheric conditions that traps  
493 pollutants in the shallow atmospheric boundary layer (ABL), leading to strengthened hazy

494 conditions in the IGP (Girolamo et al., 2004; Gautam et al., 2007). The outflow of aerosols to  
495 the Bay of Bengal is clearly depicted by satellite data. As shown in the first column of Fig. 7b,  
496 however, only the HAD model shows the observed spatial pattern and magnitude of AOD,  
497 although it overestimates AOD over eastern IGP. Other models greatly underestimate the high  
498 AOD over IGP by 50% on average. In addition, the observed north-south gradient of AOD is  
499 not captured by most models, with SPR showing no gradient and ECH and GIM showing  
500 opposite gradient. The model underestimation over the Indian subcontinent in winter is  
501 probably owing to missing aerosol species such as nitrate aerosol suggested by Fig. 6,  
502 incorrect meteorological fields such as air temperature and relative humidity, or the  
503 underestimation of anthropogenic emissions (discussed in more details in Section 6).

504 Starting from the pre-monsoon season (MAM), the entire South Asia is characterized by  
505 high AOD mainly due to the mineral dust transported from the arid and desert regions in  
506 southwest Asian dust sources by westerly winds, with maximum AOD over western IGP seen  
507 from most satellites (Fig. 7a). As shown in the second column of Fig. 7b, five models (GOC,  
508 SPR, GIM, GIE and GE5) partially capture this observed spatial distribution and magnitude.  
509 However, the HAD model shows high biases of AOD over northern India due to nitrate (refer to  
510 Fig. 6). A higher nitrate concentration than dust is unrealistic because the contribution of dust  
511 to the total AOD has been reported to be over 60% during pre-monsoon season by Srivastava  
512 et al. (2012a) based on the ground based sun/sky radiometer data. The dust source in the  
513 northwestern parts of South Asia is weak in HAD (Fig. 7b). Additionally, the ECH model shows  
514 very low AOD and little dust over IGP associated with its small dust size in coarse mode (Table  
515 1). Despite these deficiencies, model simulations over South Asia during the pre-monsoon  
516 season are still closer to the satellite data than those during winter, with the model-averaged  
517 AOD capturing 65% of the satellite data in the pre-monsoon season compared to only 50% in  
518 winter.

519 During the monsoon season (JJAS), dust transported from the Arabian Peninsula by the  
520 strong southwesterly winds explains the high AOD over northwestern India. High AOD over the  
521 Arabian Sea and southwest Asia is evident in MODIS and MISR (Fig. 7a). As shown in the  
522 third column of Fig. 7b, most models reproduce both the spatial distribution and the magnitude  
523 of AOD during this season, implying that these models capture dust emission over the Arabian  
524 Peninsula and its transport to South Asia. However, it should be noted that during the  
525 monsoon season the monthly mean AOD from MODIS is likely to be biased high as shown  
526 earlier in Fig 5, partly due to underestimated surface reflectance.

527 During the post-monsoon season (ON), the southwesterly flow significantly weakens,  
528 and thus dust transported to the Indian subcontinent is lower compared to the pre-monsoon  
529 and monsoon seasons. Based on the spatial distributions from satellite data (Fig. 7a), high  
530 AOD is found along IGP with maxima over western IGP including Punjab, Haryana and  
531 western Uttar Pradesh that are associated with biomass burning from agriculture waste fires.  
532 With the aid of northwesterly winds, aerosols are transported to the central IGP along the  
533 valley as well as the region to the south (Badarinath et al., 2009a, b). However, none of the  
534 models capture these features (the fourth column of Fig. 7b), indicating the biomass burning

535 emissions are severely underestimated in the current inventory based on GFED2, which will be  
536 discussed further in Section 6.4. In contrast to the underestimations by other models, HAD  
537 overestimated AOD over IGP due to the high amount of nitrate (Fig. 6).

538

#### 539 **4.4 Aerosol vertical distribution**

540 Figure 8 shows the comparison of aerosol extinction profile among models and with CALIOP  
541 data in four seasons. In order to represent the latitudinal gradient of aerosol vertical profiles,  
542 two locations are chosen, Kanpur in northern India and Hyderabad in central India (refer two  
543 locations to Fig. 1). The CALIOP aerosol extinction profile over Kanpur (Fig. 8a,  $2^\circ \times 2^\circ$  box  
544 averaged around the station location) reaches a maximum value of  $0.4 \text{ km}^{-1}$  at the altitude  $< 1$   
545 km during winter ( $Z_a=1.18 \text{ km}$ ) but decreases rapidly upward and diminishes around 4 km.  
546 Note that low values near the surface (within 180 meters) in CALIOP profiles are likely due to  
547 the contamination by the surface return (CALIPSO, 2011; Koffi et al., 2012). In contrast with  
548 the relatively stable lower troposphere in winter, boundary layer mixing, convection, and  
549 transport are strengthened in pre-monsoon season. As a result, aerosols are more efficiently  
550 mixed vertically, with  $Z_a$  from CALIOP almost doubled from the season of DJF to MAM (from  
551 1.18 to  $2.18 \text{ km}$ ). The aerosol vertical mixing is relatively uniform within the lowest 2 km and  
552 extends to higher altitude around 6 km in MAM. The aerosol extinction near the surface in  
553 MAM is only 60% of its DJF values with the fraction of AOD in the lowest 2 km reducing from  
554 84% in DJF to 52% in MAM. The aerosol profile during monsoon season (JJAS) is similar to  
555 that in pre-monsoon period but with a slightly lower value of  $Z_a$  as  $2.02 \text{ km}$ ; and the profile  
556 during the post-monsoon is similar to that in the winter but with a slightly higher value of  $Z_a$   
557 as  $1.24 \text{ km}$ .

558 Most models, especially GE5, capture the observed seasonal variation of  $Z_a$  (and  $F_{2\text{km}}$ )  
559 over Kanpur, with lower  $Z_a$  (higher  $F_{2\text{km}}$ ) during wintertime (DJF) and post-monsoon season  
560 (ON), while higher  $Z_a$  (lower  $F_{2\text{km}}$ ) during the pre-monsoon (MAM) and monsoon seasons  
561 (JJAS). The profiles and magnitude in models, however, are quite different from those of  
562 CALIOP. At Kanpur in DJF, most models (except for HAD and GIE) largely underestimate  
563 AOD by 59% (ECH) to 85% (SPR), consistent with the preceding results (Fig. 5-7). In particular,  
564 the extinction coefficient in the lowest 2 km is largely underestimated, with  $F_{2\text{km}}$  varying from  
565 68% (GIM) to 87% (GE5) among these five models in contrast to 84% in CALIOP (Fig. 8a). At  
566 Hyderabad in central India (Fig. 8b), models agree better with the CALIOP during the winter  
567 (DJF) and post-monsoon (ON) seasons. At both stations, models agree better with CALIOP  
568 during the dust-laden pre-monsoon (MAM) and monsoon (JJAS) seasons than during two  
569 other seasons, consistent with the results in Fig. 7a-b. There are some extremes of model  
570 simulated vertical profiles. For example, HAD produces extremely high extinction coefficients  
571 close to the surface at Kanpur throughout all seasons that are a factor of two greater than  
572 CALIOP in the season of DJF and a factor of ten greater in ON; GIE and GIM are greater than  
573 CALIOP by a factor of four and seven close to the surface in JJAS, respectively; and GIE  
574 exhibits extremely large extinction coefficients between 2 and 3 km in all seasons, which is not  
575 found in CALIOP.

576

577 **4.5 Monthly BC surface concentration**

578 Figure 9 shows the observed and modeled monthly surface BC concentration in the year of  
 579 2006 (2005 from model ECH) at eight ICARB stations (refer the locations to Fig.1). In general,  
 580 the magnitude of BC surface concentrations is closely related to the strength of emission  
 581 source, with higher values in northern India where higher BC anthropogenic emissions are  
 582 located (refer the spatial pattern to Fig.2). The highest BC surface concentration is particularly  
 583 found in the largest Indian city Delhi, with a value of  $27\mu\text{g m}^{-3}$  in January. In contrast, BC  
 584 surface concentration is lower in the remote sites, such as the island sites (Minicoy and Port  
 585 Blair) and mountain site (Nainital), not exceeding  $2.8\mu\text{g m}^{-3}$ . The observed surface BC  
 586 concentration exhibits pronounced seasonal variation with higher values found in the winter  
 587 and post-monsoon seasons and lower values in the spring and summer, which can be  
 588 attributed to the seasonal variations of emission, atmospheric boundary layer (ABL) depth  
 589 (affecting vertical mixing), and rainfall (removing BC from the atmosphere). It was reported by  
 590 previous studies that total BC loading over South Asia mainly resulted from biofuel emissions  
 591 in winter along with coal burning in the vicinity of the measurement location (e.g. Ali et al.,  
 592 2004; Singh et al., 2008; Beegum et al., 2009; Srivastava et al., 2012b). In comparison with  
 593 observation, modeled BC surface concentrations at all stations except Nainital (a mountain  
 594 site) and Kharagpur are too low, especially in winter. In particular, at Delhi and Hyderabad -  
 595 two very large cities with populations of 16.75 and 6.81 million respectively (Table 1), all  
 596 models show a pronounced low bias in the winter, capturing only 3%-19% of the observed  
 597 values. As a matter of fact, the models have difficulties to reproduce the observed high  
 598 pollution levels only near the emission sources such as urban cities (e.g. Delhi and  
 599 Hyderabad), but also in more remote locations (e.g. over the mountain site of Nainital and the  
 600 island sites of Minicoy and Port Blair). At Minicoy and Port Blair, where the observed BC  
 601 concentrations are relatively low, models capture only about 10%-38% of the observed values.  
 602 In addition to the fact that modeled AODs were also found to be significantly low in comparison  
 603 with both AERONET point observations and with the multiple gridded satellite data from  
 604 MODIS, SeaWiFS (both  $1^\circ \times 1^\circ$  resolution) and MISR ( $0.5^\circ \times 0.5^\circ$  resolution) on regional scales,  
 605 as shown earlier in Fig. 5 and Fig. 7, the underestimations of modeled BC and AOD in winter  
 606 are more likely due to other factors than coarse model resolution, which will be discussed in  
 607 details in Section 6. As an exception, the simulated BC surface concentrations are found to  
 608 have a better agreement at Kharagpur, a semi-urban city with populations less than 1 million,  
 609 where models capture 20%-100% of the observed value. This contrast with other stations is  
 610 possibly attributed to the fact that BC loading at Kharagpur mainly comes from coal-fired power  
 611 plants (Nair et al., 2007), which are likely well represented in the emission data (discussed  
 612 further in Section 6.3).

613

614 **5. Model diversity**

615 Clearly, there is a large diversity existing among models in simulating AOD and BC  
 616 concentrations as shown in Fig. 4-9, despite similar emission datasets used in these models  
 617 (see Section 2.2 and Table 1). It is seen that models with the same emissions datasets

618 produce quite different results. For example, at Kharagpur, shown in the upper right panel of  
619 Fig.9, the surface concentration of BC from the SPR model is four times as large as that from  
620 GIM, although both models use the same anthropogenic emission (A2-ACCMIP) and biomass  
621 burning emission (GFED2). Similarly, surface concentration of BC in the HAD model is twice  
622 as that of GOC, although the same emissions (A2-MAP and GFED2) are used in both models.  
623 Such substantial differences indicate that the large diversity among model simulations is due to  
624 factors other than the differences in emissions. Textor et al. (2007) also found that the  
625 differences in the model treatment of atmospheric processes (e.g., wet removal, dry deposition,  
626 cloud convection, aqueous-phase oxidation and transport), assumptions of particle size,  
627 mixture, water uptake efficiency, and optical properties are more responsible than emission for  
628 the model diversity.

629 The multi-model diversity (defined as the percentage of the standard deviation to the mean  
630 of results from the seven models) over South Asia in 2006 (2005 from the model ECH) is  
631 summarized in Table 3 (also demonstrated in supplement Fig. S1-3). In general, on an annual  
632 basis, we found the following features: (1) For aerosols with anthropogenic origin (i.e. BC, OA  
633 and SO<sub>4</sub>), the diversity of dry deposition among models is large, with diversity ranging from  
634 41% to 46% across these three species. Correspondingly, the fraction of dry deposition to total  
635 deposition shows 29-40% diversity for the same three species. In contrast, the diversity of wet  
636 deposition is relatively smaller with a range from 15 to 22% across these three species. The  
637 chemical production of sulfate in gas phase among models (four models) has large diversity  
638 about 66%. (2) For mineral dust, the emission itself has very large diversity among the models  
639 about 124%, leading to a similarly large diversity of dry deposition (aerodynamic dry deposition  
640 + gravitational settling) of 115%. The difference of treatment of dust size bin in models  
641 contributes significantly to these diversities (see Table 1). In contrast, diversity of dust mass  
642 loading and AOD are much smaller at 45% and 22% respectively. (3) BC has the largest  
643 model diversity of mass extinction efficiency (MEE) at 51%, compared to 25% and 27% for  
644 SO<sub>4</sub> and OA respectively.

645 It is noted that the function of Table 3 is to quantify the diversity of these models over  
646 South Asia instead to reveal the discrepancies of models from observations. SO<sub>4</sub> and dust are  
647 the major contributors to the total AOD in Table 3. However, this result is only based on the  
648 models, and thus it does not necessarily mean that the contribution of OA is lesser in the  
649 observation. For instance, the simulated AOD from OA is only 1/3 of that from SO<sub>4</sub> averaged  
650 over South Asia (Table 3). However, OA likely contributes more to the total observed AOD  
651 than SO<sub>4</sub> does, indicated by its larger (exceeding twice) observed surface concentration at  
652 stations along IGP as shown in the following section. Unfortunately, we cannot quantify the  
653 relative contribution of individual aerosol species to total AOD in observations because we  
654 have limited ability to separate the individual AOD from the total.

655 We further examine the aerosol refractive index at the wavelength of 550nm for each  
656 species as listed in Table 1. The real parts of refractive indices (representing phase velocity) at  
657 550nm are similar among the seven models, but the imaginary parts (representing light  
658 absorption) are different. In the case of BC, the most absorbing aerosol, the imaginary parts of

Xiaohua 4/15/2015 11:26 AM

**Deleted:** More recently, Bond et al. (2013) pointed out that large differences in modeled horizontal and vertical transport are mostly responsible for the inter-model diversity of BC distributions.

Xiaohua 4/15/2015 1:00 PM

**Deleted:** is

Xiaohua 4/15/2015 1:02 PM

**Deleted:** is

Xiaohua 4/15/2015 1:44 PM

**Deleted:** its

refractive indices are 0.44 in four models (HAD, GOC, SPR, GE5) and 0.71 in three models (ECH, GIE, GIM). For dust, the light absorption at 550nm is significantly less than that of BC. The imaginary refractive index of dust ranges from 0.001 (ECH) to 0.008 (GE5), a range that is much wider than that of BC. In order to test the sensitivity of MEE and mass absorption efficiency (MAE) to the values of the real and imaginary refractive indices, we conduct Mie calculation for BC and dust at 550 nm in several cases in which the different real and imaginary parts of refractive indices are combined (see supplementary Table S1 and S2). As for BC, we find that MEE and MAE enhance by ~40% from CASE 1 (representing the models HAD, GOC, SPR, GE5) to CASE 2 (representing the models ECH, GIE, GIM) with increasing both the imaginary and real parts. However, it is not necessary that the models in CASE 2 simulate higher AOD. For example, the model HAD shows higher AOD than the model ECH although the latter has higher real and imaginary parts (Fig. 4a and b). Therefore, this clearly suggests that there are other factors involved such as meteorology and emissions. Bond and Bergstrom (2006) attempted to increase BC imaginary part to 0.79, but this effort alone cannot remove the low bias of AAOD and AOD in models as suggested by this study. Bond et al. (2013) also pointed out that large differences in modeled horizontal and vertical transport are mostly responsible for the inter-model diversity of BC distributions. As for dust, we find that the MEE and MAE of dust are insensitive to the change of imaginary part, but sensitive to the change of real part. Dust is minimal in the post-monsoon and the Winter seasons when the largest discrepancy occurs in models, however, small changes in the values of imaginary and real parts of refractive indices of dust would not impact much on AOD and AAOD simulations. Again, other factors such as meteorology and emissions are more likely dominant. The differences in the absorption properties, together with the differences of model simulated BC and dust amount, contribute to the diversity of model calculated AAOD at 37%.

## 6. Possible causes of model underestimation of aerosols over South Asia

As shown in Section 4, AOD, AAOD and BC surface concentration over South Asia are consistently underestimated in seven global models used in this study, in particular during winter and the post-monsoon season. Such underestimation seems to be a common problem in other models as well (e.g. Reddy et al., 2004; Ganguly et al., 2009; Nair et al., 2012). AOD and surface BC concentrations are most severely underestimated over the IGP (the main region of anthropogenic emissions). Several possible causes for these underestimations are suggested below.

### 6.1 Wintertime relative humidity (RH) over the IGP

Foggy days with high near-surface relative humidity are very common during wintertime over IGP (Gautam et al., 2007). For example, Kanpur was subjected to heavy fog or haze for about >65% days in December 2004, with averaged surface RH of about 75% and the surface temperature about 14.6°C (Tripathi et al., 2006). Low precipitation and thus low wet removal in winter further contributes to accumulation of aerosols (Tripathi et al., 2006).

Xiaohua 4/15/2015 1:04 PM  
Deleted: ex  
Xiaohua 4/15/2015 1:05 PM  
Deleted: is  
Xiaohua 4/15/2015 1:06 PM  
Deleted: , which are lower than the value of 0.79 recommended by Bond and Bergstrom (2006)

712       Figure 10 shows comparisons between models and in-situ measurements (ISRO-GBP  
713 land campaign) at four stations located in the IGP region in December 2004. Comparisons are  
714 shown for surface meteorological conditions (RH and temperature); surface aerosol  
715 concentrations of  $\text{SO}_4^{2-}$ ,  $\text{NO}_3^-$ , OA and BC; and columnar AOD and AAOD. AODs from the  
716 models are only 10% to 50% of the observed values at Kanpur. Interestingly, we found that RH  
717 in six of the seven models (except for HAD) only range from 11 to 35% at Kanpur, much lower  
718 than the measured RH of 75% (first row, Fig. 10). This large underestimation of RH could be  
719 partly due to the warm bias of air temperature by 1.7-7.5 °C across models (second row, Fig.  
720 10) and thus high bias of saturation water vapor pressure and low bias of RH. Under such dry  
721 conditions in models, the hygroscopic growth of soluble aerosols is consequently suppressed.  
722 Averaged over these four IGP stations, for example, if RH is improved from the modeled 21%  
723 to the observed 66%, mass extinction efficiencies (MEE) of  $\text{SO}_4^{2-}$  would be doubled, and those  
724 of OC and  $\text{NO}_3^-$  would be enhanced by 50% (Fig. 11). It is interesting that the HAD model, in  
725 which the simulated AOD matches observed one relatively better, is the only model with high  
726 bias of RH.

727       In addition to favor hygroscopic growth, foggy conditions also favor the formation of  
728 secondary inorganic aerosol through the aqueous-phase reactions. This phenomenon was  
729 supported by the observations of increased aerosol number concentration and surface  $\text{SO}_4^{2-}$   
730 concentrations under foggy conditions at Kanpur (Tare et al., 2006), Hisar and Allahabad (Ram  
731 et al., 2012a). High RH and lower temperature in winter also favor the formation of  $\text{NH}_4\text{NO}_3$  by  
732 the reaction of nitric acid ( $\text{HNO}_3$ ) with  $\text{NH}_3$  (Feng and Penner 2007; Ram et al., 2010b; Ram et  
733 al., 2012b). However, the lack of representing foggy conditions in current models, which is  
734 indicated by the low bias of RH, would suppress these reactions in winter. Hence, it is not  
735 surprising that the surface mass concentrations of  $\text{SO}_4^{2-}$  and  $\text{NO}_3^-$  in models are found to be  
736 much lower than the observed values. As shown in Fig. 10, all models underestimate the  
737 surface concentration of  $\text{SO}_4^{2-}$ , with capturing merely from 5% (GIE and GIM) to 50% (GE5) of  
738 the observed value.  $\text{SO}_4^{2-}$  concentration, however, is found low in HAD as well although with  
739 high relative humidity. The specific reason is unclear yet. Among three models that include  
740  $\text{NO}_3^-$ , GIE and GIM produce extremely low  $\text{NO}_3^-$  concentrations that are only 0.1% of the  
741 observed amount, whereas HAD captures about 38% of the observation. The model  
742 underestimations of surface aerosol concentrations might be caused by other factors as well,  
743 such as unaccounted for anthropogenic emissions (see section 6.3) or insufficient oxidant  
744 amounts ( $\text{H}_2\text{O}_2$  and OH); however, the lack of representing foggy conditions or the low bias of  
745 RH in the models appears to be a critical factor contributing to the overall underestimation of  
746 aerosols.

## 747 **6.2 Nitrate component**

748       As shown in Fig. 10, the observed surface concentrations of  $\text{NO}_3^-$  are comparable to or even  
749 higher than those of  $\text{SO}_4^{2-}$  at four stations (e.g.  $14.9 \mu\text{g m}^{-3}$  of  $\text{SO}_4^{2-}$  and  $15.7 \mu\text{g m}^{-3}$  of  $\text{NO}_3^-$  at  
750 Kanpur, and  $14.1 \mu\text{g m}^{-3}$  of  $\text{SO}_4^{2-}$  and  $31.4 \mu\text{g m}^{-3}$  of  $\text{NO}_3^-$  at Agra). However,  $\text{NO}_3^-$  is either  
751 missing in the models (GOC, ECH, SPR, GE5) or much too low (especially in GIE and GIM).

753 Interestingly, AOD is closer to observations in the HAD model than in other models, which is  
754 not only apparent at 4 stations in IGP (Kanpur, Agra, Allahabad and Hisar) (Fig. 10) but also  
755 over entire South Asia (Fig. 7b). Such agreement is partly associated with its inclusion of  $\text{NO}_3^-$   
756 (Fig. 6) and aforementioned high relative humidity in winter (Section 6.1). This study  
757 underscores the importance of  $\text{NO}_3^-$  to adequately represent the total AOD over South Asia.  
758

### 759 **6.3 Anthropogenic/Biofuel emission amounts and seasonal variation**

760 The uncertain and inadequate representations of aerosol emissions over South Asia have  
761 been pointed out by previous studies (e.g. Sahu et al., 2008; Ganguly et al., 2009; Nair et al.,  
762 2012; Lawrence and Lelieveld, 2010). The results in this study further prove this issue. At  
763 Kanpur, the models underestimate not only surface concentrations of  $\text{SO}_4^{2-}$  and  $\text{NO}_3^-$  as  
764 discussed earlier but also those of OA and BC, with capturing only 8% (GIE and GIM) to  
765 75% (SPR) of the observed OA values, and 8% (GIE and GIM) to 46% (SPR) of the observed  
766 BC values, respectively. At other stations in the IGP such as Agra, Allahabad and Hisar (Fig.  
767 10), the surface concentrations of OA, BC,  $\text{SO}_4^{2-}$  and  $\text{NO}_3^-$  are underestimated in a similar  
768 degree by all models, although these stations are less populated than Kanpur. AOD and  
769 AAOD, indicating columnar aerosol loading, are also underestimated by all these models. It is  
770 well known that air pollutants are confined to near surface in winter due to the low ABL,  
771 thereby the results above suggest that the anthropogenic emissions used by the models (i.e.,  
772 A2-ACCMIP and A2-MAP) are likely biased low. BC emissions in year 2000 over India from  
773 A2-ACCMIP and A2-MAP are  $0.5 \text{Tg yr}^{-1}$ , which is at the low end of a group of emission  
774 inventories, for instance, lower than those considered by REAS and GAINS-2008 emission  
775 inventories (Fig. 5a in Granier et al., 2011) by 40% or  $0.3 \text{Tg yr}^{-1}$ . With the REAS emission  
776 inventory, Nair et al. (2012) reported that the simulated BC surface concentration agreed better  
777 with observations at Kharagpur.

778 Different from other regions in northern hemisphere where fossil fuel burning and industrial  
779 processes tend to dominate, biofuel and open biomass burning in South Asia contribute two-  
780 thirds of carbon-containing aerosols to form the dense brown clouds in winter (Gustafsson et  
781 al., 2009). Over India, 42% of total BC emission is from biofuel, which is believed to be the  
782 largest source of BC, with the remaining 33% from open biomass burning and 25% from fossil  
783 fuel (Venkataraman et al., 2005). The percentage of biofuel is high because residential heating  
784 and cooking (burning of wood, paper or other solid wastes) is quite common in South Asia,  
785 especially among the underprivileged, leading to large amount of smoke comprised mainly of  
786 black carbon and condensed semi-volatile organics. Based on in-situ measurements, the ratios  
787 of OC/BC surface concentrations were reported as high as  $8.0 \pm 2.2$  at Allahabad (Ram et al.,  
788 2012a) and  $8.5 \pm 2.2$  at Hisar (Rengarajan et al., 2007) in December 2004, indicating a major  
789 emission source from biomass combustion including biofuel and open biomass burning  
790 (Husain et al., 2007). However, in this study, fossil fuel are the dominant emission sources  
791 instead, because the ratio of OC/BC anthropogenic emission (from combination of fossil fuel  
792 and biofuel) in A2-ACMMIP (A2-MAP) emission database is 3.2 (2.6) (see Section 2.2) over  
793 South Asia, and thus it is not surprising that the ratios of OC/BC surface concentrations are

794 found only varying 0.4-4.0 across models at Allahabad and 0.6-3.8 at Hisar. Although the ratio  
795 of OC/BC in open biomass burning emission database is higher with a value of 8.0, open  
796 biomass burning emissions are very low in winter, only 4% of anthropogenic emissions (see  
797 Fig.2 and Fig.3). Furthermore, we found that the simulated BC surface concentrations by most  
798 models agree better with the observations at Kharagpur than at other stations (Fig. 9). As  
799 reported by Prasad et al. (2006), the sources of BC at Kharagpur located in eastern IGP were  
800 mainly linked to the clusters of the coal-based industries there. Therefore, this contrast  
801 suggests that the fossil fuel emissions are likely better represented than the biofuel emissions  
802 in the A2-MAP and A2-ACCMIP emission inventories. In addition, the lack of seasonal  
803 variation in anthropogenic emission datasets would amplify the underestimation of aerosol  
804 amount during the winter when biofuel emissions are prevalent. In sum, the model  
805 underestimation of anthropogenic OA and BC concentrations in winter is mostly due to the  
806 underestimation of biofuel emissions.  
807

#### 808 **6.4 Agriculture waste burning emissions**

809 During the post-monsoon season (October-November), the extensive agriculture waste  
810 burning after harvest in northwest India (e.g., Punjab) makes a large contribution to the dense  
811 haze over South Asia based on previous observational studies (Vadrevu et al., 2011; Sharma  
812 et al., 2010). The agricultural fires in this area are evident in the MODIS fire count product.  
813 Smoke plumes from Punjab also impact the downwind regions by eastward transport along  
814 IGP and southward to central-south India (Sharma et al., 2010; Badarinath et al., 2009a, b).

815 Over India, the contribution from open biomass burning to the total BC emission is  
816 significant, about half of anthropogenic emissions (i.e. biofuel plus fossil fuel emissions)  
817 (Venkataraman et al., 2005). The biomass burning contribution is evident based on the  
818 AERONET data at Lahore, where AAOD enhances by 70% in November (after harvest) from  
819 previous months (Fig. 5), and its contribution is also clearly seen in the MODIS-Terra and  
820 Aqua data with the maximum AOD found near Lahore in the post-monsoon season (the fourth  
821 column of Fig. 7a). BC emission from open biomass burning (based on GFED2) used by the  
822 models, however, is less than 1% of that from anthropogenic sources (comparing Fig. 2 and  
823 Fig. 3) during the post-monsoon season, both on regional average and in areas around Lahore,  
824 Therefore, it is not surprising that all models fail to capture high AAOD and AOD in this season  
825 (Fig. 5 and Fig. 7b). The underestimation of BC emission from agriculture waste burning also  
826 implies a similar degree of underestimation of OC from the same source.

827 The open biomass burning emission from GFED2 is derived from MODIS burned area  
828 products. It was previously reported that the small fires such as agricultural waste burning  
829 were largely missing in the GFED product (e.g. van der Werf et al., 2010; Randerson et al.,  
830 2012). The agricultural waste burning area is usually underestimated or overlooked in MODIS  
831 because the size of agriculture fires is too small to generate detectable burn scars in the 500  
832 meter pixel resolution of MODIS product (van der Werf et al., 2010; Randerson et al., 2012).

#### 834 **6.5 Other factors**

835 Other factors can also cause the models to underestimate AOD. For example, the observed  
836 ratio of secondary organic carbon (SOC) to primary OC is 30% - 40% in several stations  
837 located in North India, suggesting a significant contribution from SOC (Rengarajan et al., 2007;  
838 Ram and Sarin et al., 2010a). However, only two models include a resolved SOC chemistry. In  
839 addition, although the dust emission is minimal in winter compared to anthropogenic emission,  
840 dust sources from road traffic, soil re-suspension, and construction activity in the urban regions  
841 of the IGP (Tripathi et al., 2006; Tiwari et al., 2009) could be important, which are not  
842 considered in the current models.

843 Some difficulties with the models might be associated with the coarse spatial resolution  
844 (at  $1.1^\circ$  –  $2.8^\circ$ , see Table 1). Considering the complex terrain variations over South Asia,  
845 especially the valley-type topography of the IGP region with the towering Himalaya in the north  
846 (Fig. 1), the aerosol processes may not be adequately represented at such coarse spatial  
847 resolution. In addition, because of the non-linearity of wind-dependent dust emission and RH-  
848 dependent aerosol hygroscopic growth, a finer model spatial resolution would result in a higher  
849 dust emission and AOD (Bian et al., 2009).

850 Another important factor contributing to high surface aerosol concentrations in winter  
851 over South Asia is the shallow wintertime ABL that suppresses ventilation thereby trapping  
852 pollutants near the surface. At Kanpur, ABL height is about 200 m in winter according to the  
853 observations (Tripathi et al., 2006; Nair et al., 2007). However, the averaged ABL in GOC and  
854 GE5 models are 400-500 m in the study region (other models did not provide this information),  
855 allowing more efficient vertical mixing to dilute the surface concentrations and thus contributing  
856 to the low bias of surface aerosol concentration (Fig. 9 and 10). Therefore, a better-  
857 constrained ABL would be helpful to reduce the model bias of surface concentrations. Here we  
858 would like to iterate, however, that the columnar AOD and AAOD during wintertime is  
859 underestimated by the models as well, despite to a lesser degree than the underestimation of  
860 surface concentration (for example, model-simulated BC concentrations are too low by a factor  
861 of about 10, compared to the underestimation of AAOD by a factor of  $\sim 3$ ). Considering the  
862 results that both aerosol surface concentration and columnar loading are underestimated, the  
863 dominant factor in underestimating aerosol surface concentrations by these models is likely the  
864 underestimation of the emissions in wintertime, as addressed in Section 6.3.

## 865 7. Conclusions

866 In this study, the aerosol simulations for 2000-2007 from seven global aerosol models are  
867 evaluated with satellite data and ground-based measurements over South Asia, in particular  
868 over IGP, one of the heavily polluted regions in the world. The high AOD over IGP is  
869 associated with persistent high aerosol and precursor gas emissions (such as dust,  $\text{SO}_2$ ,  $\text{NO}_x$ ,  
870  $\text{NH}_3$ , OA and BC) from local and upwind regions, and with its valley-type topography (bounded  
871 by the towering Himalaya) that is conducive to trapping both anthropogenic and dust aerosols  
872 in this region. The main results of this study are summarized below.

- 873 1. Averaged over the entire South Asia for 2000-2007, the annual mean AOD is about 0.27-  
874 0.33 from satellites retrievals. Six out of seven global models consistently underestimate  
875 the annual mean AOD by 15%-44% compared to MISR, the lowest bound of four satellite

877 datasets used in the present study. The model performances are worse over northern India.  
878 In general, the underestimation of aerosol loading is mainly found during the winter and  
879 post-monsoon months when anthropogenic and open biomass burning emissions are  
880 dominant.

- 881 2. During wintertime (DJF), six out of seven models largely underestimate columnar AOD and  
882 AAOD over Indian subcontinent, and the underestimations of aerosol extinction generally  
883 occur in the lower troposphere (below 2 km). The simulated surface mass concentrations of  
884  $\text{SO}_4^{2-}$ ,  $\text{NO}_3^-$ , OA and BC are as small as 0.1-60% of the observed values in winter. Several  
885 possible causes for the common underestimations are identified: (a) the wintertime near-  
886 surface relative humidity is too low (e.g., about 20% in IGP in six out of seven models,  
887 compared to the observed value of > 60%) such that the hygroscopic growth of soluble  
888 aerosols and formation of secondary inorganic aerosol ( $\text{NO}_3^-$  and  $\text{SO}_4^{2-}$ ) are suppressed;  
889 (b)  $\text{NO}_3^-$  is either missing or inadequately accounted for; (c) anthropogenic emission,  
890 especially from biofuel in winter, is underestimated in the emission datasets. The lack of  
891 seasonal variation of emissions amplifies the discrepancies in winter.  
892 3. During the post-monsoon season (ON), none of the models capture the observed high  
893 AOD over western and central IGP. AAOD and BC surface concentrations are  
894 underestimated at the stations in IGP as well. Such discrepancy is attributed largely to the  
895 underestimation of open biomass burning in the satellite-based emission inventory  
896 (GFED2). It is likely due to missing small agricultural waste burning that is difficult to be  
897 retrieved by the satellite remote-sensors.  
898 4. As for the inter-model diversity, the results show that the largest diversity occurs in the  
899 treatment of dry deposition, with diversity of dry deposition amount ranging from 41 to 46%  
900 for BC, OA, and  $\text{SO}_4^{2-}$ . In contrast, the diversity of wet deposition is smaller, from 15 to 22%  
901 across three species. For mineral dust, the emission itself has very large diversity among  
902 the models (about 124%), leading to a similar diversity of dry deposition (aerodynamic dry  
903 deposition + gravitational settling) as of 115%, although the diversity of dust AOD is much  
904 smaller at 22%.

905 To sum up, we have identified the major discrepancies of seven state-of-the-art global  
906 aerosol models in simulating aerosol loading over South Asia. Results from this study suggest  
907 directions to improve model simulations over this important region, including improving  
908 meteorological fields (particularly relative humidity), revising biofuel and agriculture fire  
909 emission inventories, and adding/improving  $\text{NO}_3^-$ . Currently, we are working on quantifying the  
910 factors that cause the model underestimation by ranking their importance via a series of model  
911 sensitivity experiments using the GEOS5 model, [which is difficult for multi-models used in this](#)  
912 [study owing to the limitation of model outputs](#). Our ongoing work includes adjusting the model  
913 spatial resolution, emission strength, and meteorological variables and adding nitrate, which  
914 will be presented in subsequent publications. Here, we also would like to suggest to  
915 establish more systematic measurements, especially long-term (at least one year-around)  
916 surface and vertical characterization of aerosol composition, precursor gases, optical

917 properties, and meteorological fields (e.g. temperature, winds, and relative humidity), because  
918 they are essential for understanding the aerosol physical and chemical characterization.  
919

## 920 Acknowledgement

921 We thank the ICARB, ISRO-GBP, and AERONET networks for making their data available.  
922 Site PIs and data managers of those networks are gratefully acknowledged. We also thank the  
923 Goddard Earth Science Data and Information Services Center for providing gridded satellite  
924 products of SeaWiFS, MISR, and MODIS through their Giovanni website, and the AeroCom  
925 data management for providing access to the global model output used in this study. Dr.  
926 Brigitte Koffi is appreciated for providing L3 CALIOP data. [We appreciate that Dr. Hiren Jethva  
927 conducted Mie calculation for us.](#) X. Pan is supported by an appointment to the NASA  
928 Postdoctoral Program at the GSFC, administered by Oak Ridge Associated Universities  
929 through a contract with NASA. The work by MC, HB, DK, and PC are supported by the NASA  
930 MAP and ACMAP Programs. SEB and KT have been supported by the NASA MAP program  
931 (NN-H-04-Z-YS-008-N and NN-H-08-Z-DA-001-N). L. Pozzoli was supported by PEGASOS  
932 (FP7-ENV-2010-265148). ECHAM5-HAMMOZ simulations were supported by the Deutsches  
933 Klimarechenzentrum (DKRZ) and the Forschungszentrum Juelich. Resources supporting this  
934 work were provided by the NASA High-End Computing (HEC) Program through the NASA  
935 Center for Climate Simulation (NCCS) at Goddard Space Flight Center. We are grateful to two  
936 reviewers for their constructive and helpful comments.  
937

## 938 References

- 940 Ali, K., Momin, G.A., Tiwari, S., Safai, P.D., Chate, D.M., Rao, P.S.P.: Fog and precipitation  
941 chemistry at Delhi, North India. *Atmos. Environ.*, 38, 4215–4222, 2004.  
942
- 943 Badarinath, K.V.S., Kharol, S.K. and Sharma, A. R.: Long-range transport of aerosols from  
944 agriculture crop residue burning in Indo-Gangetic Plains—A study using LIDAR, ground  
945 measurements and satellite data, *J. Atmos. Sol. Terr. Phys.*, 71, 112– 120,  
946 doi:10.1016/j.jastp.2008.09.035, 2009a.  
947
- 948 Badarinath, K.V.S., Kharol,S.K., Sharma, A.R., V. Krishna Prasad: Analysis of aerosol and carbon  
949 monoxide characteristics over Arabian Sea during crop residue burning period in the Indo-Gangetic  
950 Plains using multi-satellite remote sensing datasets, *J. Atmos. Solar-Terr. Phys.*, 71, 1267 – 1276,  
951 2009b.  
952
- 953 Babu, S. S., Manoj, M. R., Moorthy, K. K., Gogoi, M. M., Nair, V. S., Kumar Kompalli, S.,  
954 Satheesh, S. K., Niranjan, K., Ramagopal, K., Bhuyan, P. K., and Singh, D.: Trends in aerosol  
955 optical depth over Indian region: potential causes and impact indicators, *J. Geophys. Res. Atmos.*,  
956 118, 11794–11806, doi:10.1002/2013JD020507, 2013.  
957
- 958 Bauer, S.E., Wright, D., Koch, D., Lewis, E.R., McGraw, R., Chang, L.-S. Schwartz, S.E. and  
959 Ruedy, R.: MATRIX (Multiconfiguration Aerosol TRacker of mIXing state): An aerosol  
960 microphysical module for global atmospheric models. *Atmos. Chem. Phys.*, 8, 6603-6035,  
961 doi:10.5194/acp-8-6003-2008, 2008.  
962
- 963 Bauer, S.E., Menon, S., Koch, D., Bond, T.C., and Tsigaridis, K.: A global modeling study on  
964 carbonaceous aerosol microphysical characteristics and radiative forcing. *Atmos. Chem. Phys.*, 10,  
965 7439-7456, doi:10.5194/acp-10-7439-2010, 2010.

- 966  
967 Beegum, S., Moorthy, S.N., Babu, K.K.,Satheesh, S.S., Vinoj,S.K., Badarinath,V., Safai,  
968 K.V.S., Devara, P.D., Singh, P.C.S., Vinod, S., Dumka U. C., Pant, P.: Spatial distribution of  
969 aerosol black carbon over India during pre-monsoon season. *Atmos. Environ.* 43, 071e1078, 2009.  
970
- 971 Bellouin, N., Rae, J., Jones, A., Johnson, C., Haywood, J. and Boucher, O.: Aerosol forcing in the  
972 Climate Model Intercomparison Project (CMIP5) simulations by HadGEM2-ES and the role of  
973 ammonium nitrate, *J. Geophys. Res.*, 116, D20206, doi:10.1029/2011JD016074, 2011.  
974
- 975 Bian, H., Chin, M., Rodriguez, J., Yu, H., Penner, J. E., Strahan, S.: Sensitivity of aerosol optical  
976 thickness and aerosol direct radiative effect to relative humidity, *Atmos. Chem. Phys.*, 9, 2375-  
977 2386, 2009.  
978
- 979 Bond, T. C., and Bergstrom, R. W.: Light absorption by carbonaceous particles: An investigative  
980 review, *Aerosol Sci. Technol.*, 40(1), 27–67, doi:10.1080/02786820500421521, 2006.  
981
- 982 Bond, TDoherty, S. J., Fahey, D. W., Forster, P. M., Berntsen, T., DeAngelo, B. J., Flanner, M.  
983 Ghan, K'archer, B., Koch, D., Kinne,Kondo, Y., Quinn, P. Sarofim, M. C., Schultz, MSchulz, M.,  
984 Venkataraman, C., Zhang, H., Zhang, S., Bellouin, N., Guttikunda, S. Hopke, P. K., Jacobson, M.  
985 Z., Kaiser, J. W., Klimont, Z., Lohmann, U., Schwarz, J. P., Shindell, D., Storelvmo, T., Warren, S.  
986 G., and Zender, C. S.: Bounding the role of black carbon in the climate system: A scientific  
987 assessment, *J.Res.*, 118, 5380–5552, doi:10.1002/jgrd.50171, 2013.  
988
- 989 CALIPSO: CALIPSO Quality Statements Lidar Level 3 Aerosol Profile Monthly Products Version  
990 Release: 1.00, 2011.  
991
- 992 Cherian, R., Venkataraman, C., Quaas, J. and Ramachandran, S.: GCM simulations of  
993 anthropogenic aerosol-induced changes in aerosol extinction, atmospheric heating and  
994 precipitation over India, *J. Geophys. Res. Atmos.*,118, 2938–2955, doi:10.1002/jgrd.50298, 2013.  
995
- 996 Chin, M., Ginoux, P., Kinne, S., Torres, O., Holben, B. N., Duncan, B. N., Martin, R. V., Logan, J.  
997 A., Higurashi, A. and Nakajima, T.: Tropospheric aerosol optical thickness from the GOCART  
998 model and comparisons with satellite and sun photometer measurements, *J. Atmos., Sci.*, 59, 461-  
999 483, 2002.  
000
- 001 Chin, M., Diehl, T., Dubovik, O., Eck, T. F., Holben, B. N., Sinyuk, A. and Streets, D. G. : Light  
002 absorption by pollution, dust and biomass burning aerosols: A global model study and evaluation  
003 with AERONET data, *Ann. Geophys.*, 27, 3439- 3464, 2009.  
004
- 005 Chin, M., Diehl, T., Tan, Q., Prospero, J. M., Kahn, R. A., Remer, L. A., Yu, H., Sayer, A. M.,  
006 Bian, H., Geogdzhayev, I. V., Holben, B. N., Howell, S. G., Huebert, B. J., Hsu, N. C., Kim, D.,  
007 Kucsera, T. L., Levy, R. C., Mishchenko, M. I., Pan, X., Quinn, P. K., Schuster, G. L., Streets, D. G.,  
008 Strode, S. A., Torres, O., and Zhao, X.-P.: Multi-decadal aerosol variations from 1980 to 2009: a  
009 perspective from observations and a global model, *Atmos. Chem. Phys.*, 14, 3657-3690,  
010 doi:10.5194/acp-14-3657-2014, 2014.  
011
- 012 Colarco, P. R., da Silva, A., Chin, M., and Diehl, T.: Online simulations of global aerosol  
013 distributions in the NASA GEOS-4 model and comparisons to satellite and ground-based aerosol  
014 optical depth, *J. Geophys. Res.*, 115, D14207, doi:10.1029/2009JD012820, 2010.  
015

- 016 Das, S. K., Jayaraman, A., and Misra, A.: Fog-induced variations in aerosol optical and physical  
017 properties over the Indo-Gangetic Basin and impact to aerosol radiative forcing, *Ann. Geophys.*, 26,  
018 1345–1354, doi:10.5194/angeo-26-1345-2008, 2008.  
019
- 020 Diehl, T., Heil, A., Chin, M., Pan, X., Streets, D., Schultz, M., and Kinne, S.: Anthropogenic,  
021 biomass burning, and volcanic emissions of black carbon, organic carbon, and SO<sub>2</sub> from 1980 to  
022 2010 for hindcast model experiments, *Atmos. Chem. Phys. Discuss.*, 12, 24895–24954, 2012.  
023
- 024 Feng, Y. and Penner, J. E.: Global modeling of nitrate and ammonium: Interaction of aerosols and  
025 tropospheric chemistry, *J. Geophys. Res.*, Vol. 112, D01304, doi: 10.1029/2005JD006404, 2007.  
026
- 027 Ganguly, D., Jayaraman, A., Rajesh, T. A. and Gadhavi, H.: Wintertime aerosol properties during  
028 foggy and nonfoggy days over urban center Delhi and their implications for shortwave radiative  
029 forcing, *J. Geophys. Res.*, 111, D15217, doi:10.1029/2005JD007029, 2006.  
030
- 031 Ganguly, D., Ginoux, P., Ramaswamy, V., Winker, D. M., Holben, B. N. and Tripathi, S. N.:  
032 Retrieving the composition and concentration of aerosols over the Indo-Gangetic basin using  
033 CALIOP and AERONET data, *Geophys. Res. Lett.*, 36, L13806, doi:10.1029/2009GL038315, 2009.  
034
- 035 Gautam, R., Hsu, N. C., Kafatos, M. and Tsay, S.-C.: Influences of winter haze on fog/low cloud  
036 over the Indo-Gangetic Plains, *J. Geophys. Res.*, 112, D05207, doi:10.1029/2005JD007036,  
037 2007.  
038
- 039 Gautam R., Hsu, N. C., Lau, W. K.-M. and Yasunari, T. J.: Satellite observations of desert dust-  
040 induced Himalayan snow darkening, *Geophys. Res. Lett.*, 40, 988–993,  
041 doi:10.1002/grl.50226, 2013.  
042
- 043 Girolamo, D. L., Bond, T. C., Bramer, D., Diner, D. J., Fettiger, F. , Kahn, R. A. Martonchik, J. V. ,  
044 Ramana, M. V., Ramanathan, V. and Rasch, P. J.: Analysis of Multi-angle Imaging  
045 SpectroRadiometer (MISR) aerosol optical depths over greater India during winter 2001–2004,  
046 *Geophys. Res. Lett.*, 31, L23115, doi:10.1029/ 2004GL021273, 2004.  
047
- 048 Goto, D., Takemura, T., Nakajima, T. and Badarinath, K. V. S.: Global aerosol model-derived black  
049 carbon concentration and single scattering albedo over Indian region and its comparison with  
050 ground observations, *Atmos. Environ.*, 45(19), 3277–3285, 2011.  
051
- 052 Granier, C., Bessagnet, B., Bond, T., D'Angiola, A., van der Gon, H. D., Frost, G. J., Heil, A.,  
053 Kaiser, J. W., Kinne, S., Klimont, Z., Kloster, S., Lamarque, J.-F., Liousse, C., Masui, T., Meleux,  
054 F., Mieville, A., Ohara, T., Raut, J. C., Riahi, K., Schultz, M. G., Smith, S. J., Thompson, A., van  
055 Aardenne, J., van der Werf, G. R., and van Vuuren, D. P.: Evolution of anthropogenic and biomass  
056 burning emissions of air pollutants at global and regional scales during the 1980–2010 period,  
057 *Climatic Change*, 109, 163–190, doi:10.1007/s10584-011-0154-1, 2011.  
058
- 059 Gustafsson, O., Krusa, M., Zencak, Z., Sheesley, R. J., Granat, L., Engstrom, E., Praveen, P. S.,  
060 Rao, P. S. P., Leck, C., and Rodhe, H.: Brown Clouds over South Asia: Biomass or Fossil Fuel  
061 Combustion?, *Science*, 323, 495–498, 2009.  
062
- 063 Henriksson, S. V., Laaksonen, A., Kerminen, V.-M., Räisänen, P., Järvinen, H., Sundström, A.-M.,  
064 and de Leeuw, G.: Spatial distributions and seasonal cycles of aerosols in India and China seen in  
065 global climate-aerosol model, *Atmos. Chem. Phys.*, 11, 7975–7990, doi:10.5194/acp-11-7975-2011,  
066 2011.

- 067  
068 Hess, M., K  opke, P., and Schult, I.: Optical properties of aerosols and clouds: The software  
069 package OPAC, B. Am. Meteorol. Assoc., 79, 831  844, doi: [http://dx.doi.org/10.1175/1520-0477\(1998\)079<0831:OPOAAC>2.0.CO;2](http://dx.doi.org/10.1175/1520-0477(1998)079<0831:OPOAAC>2.0.CO;2), 1998.
- 071  
072  
073 Holben, B.N., Eck, T.F., Slutsker, I., Tanre, D., Buis, J.P., Setzer, A., Vermote, E., Reagan, J.A.,  
074 Kaufman, Y.J., Nakajima, T., Lavenu, F., Jankowiak, I., Smirnov, A.: AERONET — a federated  
075 instrument network and data archive for aerosol characterization. *Remote Sens. Environ.* 66, 1  16,  
076 1998.
- 077  
078 Hsu, N. C., Tsay, S.-C., King, M. D., and Herman, J. R.: Deep Blue retrievals of Asian aerosol  
079 properties during ACE-Asia, *IEEE T. Geosci. Remote Sens.*, 44, 3180  3195, 2006.
- 080  
081 Hsu, N. C., Gautam, R., Sayer, A. M., Bettenhausen, C., Li, C., Jeong, M. J., Tsay, S.-C., and  
082 Holben, B. N.: Global and regional trends of aerosol optical depth over land and ocean using  
083 SeaWiFS measurements from 1997 to 2010, *Atmos. Chem. Phys.*, 12, 8037  8053,  
084 doi:10.5194/acp-12-8037-2012, 2012.
- 085  
086 Husain, L., Dutkiewicz, V. A., Khan, A. J., Chin, M., and Ghauri, B. M.: Characterization of  
087 carbonaceous aerosols in urban air, *Atmos. Envirion.*, 41, 6872  6883, 2007.
- 088  
089 Jethva, H., Satheesh, S. K., Srinivasan, J., and Krishnamoorthy, K.: How Good is the Assumption  
090 about Visible Surface Reflectance in MODIS Aerosol Retrieval over Land? A Comparison with  
091 Aircraft Measurements over an Urban Site in India, *IEEE Transactions on Geoscience and Remote  
092 Sensing*, 47(7), 2009.
- 093  
094 Kahn, R. A., W.-H. Li, C. Moroney, D. J. Diner, J. V. Martonchik, and E. Fishbein: Aerosol source  
095 plume physical characteristics from space-based multiangle imaging, *J. Geophys. Res.*, 112,  
096 D11205, doi:10.1029/2006JD007647, 2007.
- 097  
098 Kahn, R. A., Gaitley, B. J., Garay, M. J., Diner, D. J., Eck, T., Smirnov, A., and Holben, B. N.:  
099 Multiangle Imaging SpectroRadiometer global aerosol product assessment by comparison with the  
100 Aerosol Robotic Network, *J. Geophys. Res.*, 115, D23209, doi:10.1029/2010JD014601, 2010.
- 101  
102 Kaskaoutis, D. G., Singh, R. P., Gautam, R., Sharma, M., Kosmopoulos, P. G., Tripathi, S. N.:  
103 Variability and Trends of Aerosol Properties over Kanpur, Northern India Using AERONET Data  
104 (2001  10). *Environ. Res. Lett.* 7: 024003, doi: 10.1088/1748-9326/7/2/024003, 2012.
- 105  
106 Koffi, B., Schulz, M., Br  on, F.-M., Griesfeller, J., Winker, D., Balkanski, Y., Bauer, S., Berntsen, T.,  
107 Chin, M., Collins, W. D., Dentener, F., Diehl, T., Easter, R., Ghan, S., Ginoux, P., Gong, S.,  
108 Horowitz, L. W., Iversen, T., Kirkev  g, A., Koch, D., Krol, M., Myhre, G., Stier, P., and Takemura,  
109 T.: Application of the CALIOP layer product to evaluate the vertical distribution of aerosols  
110 estimated by global models: AeroCom phase I results, *J. Geophys. Res.*, 117, D10201,  
111 doi:10.1029/2011JD016858, 2012.
- 112  
113 Lau, K. M., Kim, M. K. and Kim, K. M.: Asian summer monsoon anomalies induced by aerosol  
114 direct forcing: The role of the Tibetan Plateau, *Clim. Dyn.*, 26, 855  864, 2006.
- 115

- 116 Lau, K. M., Kim, M. K., Kim, K. M. and Lee, W. S.: Enhanced surface warming and accelerated  
117 snow melt in the Himalayas and Tibetan Plateau induced by absorbing aerosols, Env. Res. Lett., 5,  
118 025204, doi:10.1088/1748-9326/5/2/025204, 2010.
- 119
- 120 Lawrence, M. G., and Lelieveld, J.: Atmospheric pollutant outflow from southern Asia: A review,  
121 Atmos. Chem. Phys., 10, 11,017–11,096, 2010.
- 122
- 123 Levy, R. C., Remer, L. A., Mattoo, S., Vermote, E. F., and Kaufman, Y. J.: Second-generation  
124 operational algorithm: Retrieval of aerosol properties over land from inversion of Moderate  
125 Resolution Imaging Spectroradiometer spectral reflectance, J. Geophys. Res., 112, D13211,  
126 doi:10.1029/2006JD007811, 2007.
- 127
- 128 Levy, R. C., Remer, L. A., Kleidman, R. G., Mattoo, S., Ichoku, C., Kahn, R., and Eck, T. F.: Global  
129 evaluation of the Collection 5 MODIS dark-target aerosol products over land, Atmos. Chem. Phys.,  
130 10, 10399–10420, doi:10.5194/acp-10-10399-2010, 2010.
- 131
- 132 Martonchik, J. V., Diner, D. J., Kahn, R., Gaitley, B. and Holben, B. N.: Comparison of MISR and  
133 AERONET aerosol optical depths over desert sites, Geophys. Res. Lett., 31, L16102,  
134 doi:10.1029/2004GL019807, 2004.
- 135
- 136 Menon, S., Koch, D., Beig, G., Sahu, S., Fasullo, J., and Orlikowski, D.: Black carbon aerosols and  
137 the third polar ice cap, Atmos. Chem. Phys., 10, 4559–4571, doi:10.5194/acp-10-4559-2010, 2010.
- 138
- 139 Moorthy, K. K., Beegum, S. N., Srivastava, N., Satheesh, S. K., Chin, M., Blond, N., Babu, S. S.  
140 and Singh, S.: Performance Evaluation of Chemistry Transport Models over India, Atmos. Environ.,  
141 71, 210–225, 2013.
- 142
- 143 Myhre, G., Samset, B. H., Schulz, M., Balkanski, Y., Bauer, S., Berntsen, T. K., Bian, H., Bellouin,  
144 N., Chin, M., Diehl, T., Easter, R. C., Feichter, J., Ghan, S. J., Hauglustaine, D., Iversen, T., Kinne,  
145 S., Kirkevåg, A., Lamarque, J.-F., Lin, G., Liu, X., Lund, M. T., Luo, G., Ma, X., van Noije, T.,  
146 Penner, J. E., Rasch, P. J., Ruiz, A., Selander, Ø., Skeie, R. B., Stier, P., Takemura, T., Tsigaridis,  
147 K., Wang, P., Wang, Z., Xu, L., Yu, H., Yu, F., Yoon, J.-H., Zhang, K., Zhang, H., and Zhou, C.:  
148 Radiative forcing of the direct aerosol effect from AeroCom Phase II simulations, Atmos. Chem.  
149 Phys., 13, 1853–1877, doi:10.5194/acp-13-1853-2013, 2013.
- 150
- 151 Nair, V. S., Moorthy, K. K., Alappattu, D. P., Kunhikrishnan, P. K., George, S., Nair, P. R., Babu, S.  
152 S., Abish, B., Satheesh, S. K., Tripathi, S. N., Niranjan, K., Madhavan, B. L., Srikant, V., Dutt, C. B.  
153 S., Badarinath, K. V. S., and Reddy, R. R.: Wintertime aerosol characteristics over the Indo-  
154 Gangetic Plain (IGP): Impacts of local boundary layer processes and long-range transport, J.  
155 Geophys. Res., 112, D13205, doi:10.1029/2006JD008099, 2007.
- 156
- 157 Nair, V. S., Solmon, F., Giorgi, F., Mariotti, L., Babu, S. S., and Moorthy, K. K.: Simulation of South  
158 Asian aerosols for regional climate studies, J. Geophys. Res., 117, D04209,  
159 doi:10.1029/2011JD016711, 2012.
- 160
- 161 Ohara, T., Akimoto, H., Kurokawa, J., Horii, N., Yamaji, K., Yan, X. and Hayasaka, T. : An Asian  
162 emission inventory of anthropogenic emission sources for the period 1980–2020, Atmos. Chem.  
163 Phys., 7, 4419–4444, 2007.
- 164
- 165 Pozzoli, L., Janssens-Maenhout, G., Diehl, T., Bey, I., Schultz, M. G., Feichter, J., Vignati, E., and  
166 Dentener, F.: Reanalysis of tropospheric sulphate aerosol and ozone for the period 1980–2005

- 167 using the aerosol-chemistry-climate model ECHAM5-HAMMOZ, *Atmos. Chem. Phys. Discuss.*, 11,  
168 10191-10263, doi:10.5194/acpd-11-10191-2011, 2011.  
169
- 170 Prasad, A. K., Singh, R. P., and Kafatos, M.: Influence of coal based thermal power plants on  
171 aerosol optical properties in the Indo-Gangetic basin, *Geophys. Res. Lett.*, 33, L05805,  
172 doi:10.1029/2005GL023801, 2006.  
173
- 174 Qian, Y., Flanner, M. G., Leung, L. R. , and Wang W.: Sensitivity studies on the impacts of Tibetan  
175 Plateau snowpack pollution on the Asian hydrological cycle and monsoon climate, *Atmos. Chem.*  
176 *Phys.*, 11, 1929–48, doi:10.5194/acp-11-1929-2011, 2011.  
177
- 178 Ram K., Sarin, M. M.: Spatio-temporal variability in atmospheric abundances of EC, OC and  
179 WSOC over Northern India, *Journal of Aerosol Science*, 41(1), 88-98, 2010a.  
180
- 181 Ram, K., Sarin, M. M., and Tripathi, S. N.: A 1 year record of carbonaceous aerosols from an urban  
182 site in the Indo-Gangetic Plain: Characterization, sources, and temporal variability, *J. Geophys.*  
183 *Res.*, 115, D24313, doi:10.1029/2010JD014188, 2010b.  
184
- 185 Ram, K., Sarin, M. M., Sudheer, A. K. and Rengarajan, R.: Carbonaceous and secondary inorganic  
186 aerosols during wintertime fog and haze over urban sites in the Indo-Gangetic Plain, *Aerosol Air*  
187 *Qual.Res.*, 12, 359–370, 2012a.  
188
- 189 Ram, K., Sarin, M.M., Tripathi, S.N.: Temporal trends in atmospheric PM2.5, PM10, elemental  
190 carbon, organic carbon, water-soluble organic carbon, and optical properties: impact of biomass  
191 burning emissions in the Indo-Gangetic Plain. *Environmental Science & Technology* 46, 686-695,  
192 2012b.  
193
- 194 Ramachandran, S., Rengarajan, R., Jayaraman, A., Sarin, M. M. and Das, S. K.: Aerosol radiative  
195 forcing during clear, hazy, and foggy conditions over a continental polluted location in north India, *J.*  
196 *Geophys. Res.*, 111, D20214, doi:10.1029/2006JD007142, 2006.  
197
- 198 Ramachandran, S., and Kedia S.: Aerosol, clouds and rainfall: inter-annual and regional variations  
199 over India, *Clim. Dyn.*, 40(7–8), 1591–1610, doi:10.1007/s00382-012-1594-7, 2013.  
200
- 201 Ramanathan, V., Crutzen, P. J., Lelieveld, J., Mitra, A. P., Althausen, D., Anderson, J., Andreae, M.  
202 O., Cantrell, W., Cass, G. R., Chung, C. E., Clarke, A. D., Coakley, J. A., Collins,W. D., Conant, W.  
203 C., Dulac, F., Heintzenberg, J., Heymsfield, A. J., Holben, B., Howell, S., Hudson, J., Jayaraman,  
204 A., Kiehl, J. T., Krishnamurti, T. N., Lubin, D., McFarquhar, G., Novakov, T., Ogren, J. A.,  
205 Podgorny, I. A., Prather, K., Priestley, K., Prospero, J. M., Quinn, P. K., Rajeev, K., Rasch, P.,  
206 Rupert, S., Sadourny, R., Satheesh, S. K., Shaw, G. E., Sheridan, P., and Valero, F. P. J.: Indian  
207 Ocean Experiment: An integrated analysis of the climate forcing and effects of the great Indio-  
208 Asian haze, *J. Geophys. Res.*, 106, 28371–28398, 2001.  
209
- 210 Ramanathan V., Chung C., Kim D., Bettge T., Buja L., Kiehl J.T., Washington W.M., Fu Q., Sikka  
211 D.R., Wild M.: Atmospheric brown clouds: impact on South Asian climate and hydrologic cycle.  
212 Proc Natl Acad Sci 102:5326–5333, DOI 10.1073/pnas.0500656102, 2005.  
213
- 214 Randerson, J. T., Chen, Y., van der Werf, G. R., Rogers, B. M., and Morton, D. C.: Global burned  
215 area and biomass burning emissions from small fires, *J. Geophys. Res.*, 117, G04012,  
216 doi:10.1029/2012JG002128, 2012.  
217

- 218 Reddy, M. S., Boucher, O., Venkataraman, C., Verma, S., Le' on, J.-F., Bellouin, N., and Pham, M.:  
219 General circulation model estimates of aerosol transport and radiative forcing during the Indian  
220 Ocean Experiment, *J. Geophys. Res.*, 109, D16205, doi:10.1029/2004JD004557, 2004.  
221
- 222 Rengarajan, R., Sarin, M. M., and Sudheer, A. K.: Carbonaceous and inorganic species in  
223 atmospheric aerosols during wintertime over urban and high-altitude sites in North India, *J.*  
224 *Geophys. Res.*, 112, D21307, doi:10.1029/2006JD008150, 2007.  
225
- 226 Safai, P. D., Kewat, S. , Pandithurai, G., Praveen, P. S., Ali, K., Tiwari, S., Rao, P. S. P.,  
227 Budhwant, K. B., Saha, S. K., Devara, P. C. S.: Aerosol characteristics during winter fog at Agra,  
228 North India. *J. Atmos. Chem.*, 61(2), 101–118, 2008.  
229
- 230 Sahu, S. K., Beig, G., and Sharma, C.: Decadal growth of black carbon emissions in India,  
231 *Geophys. Res. Lett.*, 35, L02807, doi:10.1029/ 2007GL032333, 2008.  
232
- 233 Sanap, S.D., Ayantika, D.C., Pandithurai, G., Niranjan, K.: Assessment of the aerosol distribution  
234 over Indian subcontinent in CMIP5 models, *Atmospheric Environment*, 87,123-137, 2014.  
235
- 236 Sayer, A. M., Hsu, N. C., Bettenhausen, C., Ahmad, Z., Holben, B. N., Smirnov, A., Thomas, G. E.,  
237 and Zhang, J.: SeaWiFS Ocean Aerosol Retrieval (SOAR): algorithm, validation, and comparison  
238 with other datasets, *J. Geophys. Res.*, 117, D03206,doi:10.1029/2011JD016599, 2012.  
239
- 240 Sayer, A. M., Hsu, N. C., Bettenhausen, C., and Jeong, M.-J.: Validation and uncertainty estimates  
241 for MODIS Collection 6 "Deep Blue" aerosol data, *J. Geophys. Res. Atmos.*, 118,7864–7872,  
242 doi:10.1002/jgrd.50600, 2013.  
243
- 244 Sessions, W. R., Reid, J. S., Benedetti, A., Colarco, P. R., da Silva, A., Lu, S., Sekiyama, T.,  
245 Tanaka, T. Y., Baldasano, J. M., Basart, S., Brooks, M. E., Eck, T. F., Iredell, M., Hansen, J. A.,  
246 Jorba, O. C., Juang, H.-M. H., Lynch, P., Morcrette, J.-J., Moorthi, S., Mulcahy, J., Pradhan, Y.,  
247 Razinger, M., Sampson, C. B., Wang, J., and Westphal, D. L.: Development towards a global  
248 operational aerosol consensus: basic climatological characteristics of the International Cooperative  
249 for Aerosol Prediction Multi-Model Ensemble (ICAP-MME), *Atmos. Chem. Phys.*, 15, 335-362,  
250 doi:10.5194/acp-15-335-2015, 2015.  
251
- 252 Sharma, A.R., Kharol, S.K., Badarinath, K.V.S., Singh, D.: Impact of agriculture crop residue  
253 burning on atmospheric aerosol loading — a study over Punjab State, India. *Ann. Geophys.* 28,  
254 367–379, 2010.  
255
- 256 Singh T., Khillare P.S., Shridhar V., Agarwal T.: Visibility impairing aerosols in the urban  
257 atmosphere of Delhi. *Environ Monit Assess* 141:67–77, 2008.  
258
- 259 Srivastava, A. K., Tripathi, S. N., Dey, S., Kanawade, V. P., and Tiwari, S.: Inferring aerosol types  
260 over the Indo-Gangetic Basin from ground based sunphotometer measurements, *Atmos. Res.*,  
261 109–110, 64–75, doi:10.1016/j.atmosres.2012.02.010, 2012a.  
262
- 263 Srivastava, A.K., Singh, S., Pant, P., Dumka, U.C.: Characteristics of black carbon over Delhi and  
264 Manora Peak-a comparative study. *Atmos Sci Lett* 13:223–230. doi:10.1002/asl.386, 2012b.  
265
- 266 Takemura, T., Nozawa, T., Emori, S., Nakajima, T. Y., and Nakajima,T.: Simulation of climate  
267 response to aerosol direct and indirect effects with aerosol transport-radiation model, *J.*  
268 *Geophys.Res.-Atmos.*, 110, D02202, doi:10.1029/2004jd005029, 2005.

- 269  
270 Takemura, T., Egashira, M., Matsuzawa, K., Ichijo, H., O'Ishi, R., and Abe-Ouchi, A.: A simulation  
271 of the global distribution and radiative forcing of soil dust aerosols at the Last Glacial Maximum,  
272 *Atmos. Chem. Phys.*, 9, 3061–3073, doi:10.5194/acp-9-3061-2009, 2009.  
273  
274 Tare, V., Tripathi, S.N., Chinnam, N., Srivastava, A.K., Dey, S., Manar, M., Kanawade, V.P.,  
275 Agarwal, A., Kishore, S., Lal, R.B., Sharma, M.: Measurements of atmospheric parameters during  
276 Indian Space Research Organization Geosphere Biosphere Program Land Campaign II at a typical  
277 location in the Ganga Basin: 2. Chemical properties, *J. Geophys. Res.*, 111, D23210,  
278 doi:10.1029/2006JD007279, 2006.  
279  
280 Textor, Schulz, M., Guibert, S., Kinne, Balkanski, Bauer, S., Berntsen, T., Berglen, T., Boucher, O.,  
281 Chin, M., Dentener, Diehl, T., Feichter, Fillmore, D., Ginoux, Gong, S., Grini, Hendricks, J.,  
282 Horowitz, L., Huang, P., Isaksen, I. S. A., Iversen, T., Kloster, S., Koch, D.,  
283 Kirkevåg, Kristjansson, J. E., Krol, M., Lauer, A., Lamarque, J. F., Liu, X., Montanaro, V., Myhre, G.,  
284 Penner, J. E., Pitari, G., Reddy, M. S., Seland, Ø., Stier, P., Takemura, T., and Tie, X.: The effect  
285 of harmonized emissions on aerosol properties in global models – an AeroCom experiment, *Atmos.*  
286 7, 4489–4501, doi:10.5194/acp-7-4489-2007, 2007.  
287  
288 Tiwari, S., Srivastava,A.K.,Bisht,D.S., Bano, T., Singh, S.,Behura, S., Srivastava,M.K.,Chate, D.M.,  
289 Padmanabhamurty, B.: Black carbon and chemical characteristics of PM10 and PM2.5 at an urban  
290 site of North India. *J. Atmos. Chem.* 62(3), 193–209. doi:10.1007/s10874-010-9148-z, 2009.  
291  
292 Tripathi, S. N., Tare, V., Chinnam, N., Srivastava, A. K., Dey, S., Agarwal, A., Kishore, S., Lal, R.  
293 B., Manar, M., Kanwade, V. P., Chauhan, S. S. S., Sharma, M., Reddy, R. R., Gopal, K. R.,  
294 Narasimhulu, K., Reddy, L. S. S., Gupta, S., and Lal, S.:  
295 Measurements of atmospheric parameters during Indian Space Research Organization Geosphere  
296 Biosphere Programme Land Campaign II at a typical location in the Ganga basin: 1. Physical and  
297 optical properties, *J. Geophys. Res.*, 111, D23209, doi:10.1029/2006JD007278, 2006.  
298  
299 Tsigaridis, K., Koch, D. M., and Menon, S.: Uncertainties and importance of sea-spray composition  
300 on aerosol direct and indirect effects, *J. Geophys. Res.*, 118, 220–235, doi:10.1029/2012JD018165,  
301 2013.  
302  
303 Vadrevu, K.P., Ellicott, E., Badarinath, K.V.S., Vermote, E.: MODIS derived fire characteristics and  
304 aerosol optical depth variations during the agricultural residue burning season, north India.  
305 Environmental Pollution 159, 1560–1569, 2011.  
306  
307 Vadrevu, K. P., Giglio, L., Justice C.: Satellite based analysis of fire–carbon monoxide relationships  
308 from forest and agricultural residue burning (2003–2011), *Atmos. Environ.*, 64,179-191, 2013.  
309  
310 van der Werf, G. R., Randerson, J. T., Giglio, L., Collatz, G. J., Mu, M., Kasibhatla, P. S., Morton,  
311 D. C., DeFries, R. S., Jin, Y., and van Leeuwen, T. T.: Global fire emissions and the contribution of  
312 deforestation, savanna, forest, agricultural, and peat fires (1997–2009), *Atmos. Chem. Phys.*, 10,  
313 11707–11735, doi:10.5194/acp-10-11707-2010, 2010.  
314  
315 Venkataraman, C., Habib, G., Eiguren-Fernandez, A., Miguel, A. H., and Friedlander, S. K.:  
316 Residential biofuels in south asia: Carbonaceous aerosol emissions and climate impacts, *Science*,  
317 307, 1454–1456, 2005.  
318

- 319 Venkataraman, C., Habib, G., Kadamba, D., Shrivastava, M., Leon, J.-F., Crouzille, B., Boucher, O.  
320 and Streets, D. G.: Emissions from open biomass burning in India: Integrating the inventory  
321 approach with high-resolution Moderate Resolution Imaging Spectroradiometer (MODIS) active-fire  
322 and land cover data, Global Biogeochem. Cycles, 20, GB2013, doi:10.1029/2005GB002547,  
323 2006.
- 324
- 325 Yasunari, T. J., Bonasoni, P., Laj, P., Fujita, K., Vuillermoz, E., Marinoni, A., Cristofanelli, P.,  
326 Duchi, R., Tartari, G., and Lau, K.-M.: Estimated impact of black carbon deposition during pre-  
327 monsoon season from Nepal Climate Observatory – Pyramid data and snow albedo changes over  
328 Himalayan glaciers, Atmos. Chem. Phys., 10, 6603-6615, doi:10.5194/acp-10-6603-2010, 2010.
- 329
- 330 Yu, F., Luo, G., and Ma, X.: Regional and global modeling of aerosol optical properties with a size,  
331 composition, and mixing state resolved particle microphysics model, Atmos. Chem. Phys., 12,  
332 5719-5736, doi:10.5194/acp-12-5719-2012, 2012.
- 333
- 334
- 335
- 336
- 337
- 338
- 339
- 340
- 341
- 342
- 343
- 344
- 345
- 346
- 347
- 348

349  
350  
351**Tables**

Table1. General information of models used in this study.

Model	HadGEM2	GOCART-v4	ECHAM5-HAMMOZ	GISS-modelE	GISS-MATRIX	SPRINTARS	GEOS5-GOCART
ID	HAD	GOC	ECH	GIE	GIM	SPR	GE5
Time range	2000-2006	2000-2007	2000-2005	2000-2008	2000-2007	2000-2008	2000-2008
Spatial Resolution <sup>a</sup>	1.8×1.2×38	2.5×2×30	2.8×2.8×31	2.5×2×40	2.5×2×40	1.1×1.1×56	2.5×2×72
Anthr. Emi. <sup>b</sup>	A2-MAP	A2-MAP	A2-MAP	A2-ACCMIP	A2-ACCMIP	A2-ACCMIP	A2-ACCMIP
BB Emi. <sup>c</sup>	GFED2	GFED2	GFED2	GFED2	GFED2	GFED2	GFED2
Met. Field	ERA- Interim	GEOS-DAS	ECMWF analysis	NCEP wind	NCEP-wind	NCEP/ NCAR	MERRA
Refrac- -tive	SO <sub>4</sub> <sup>2-</sup> : 1.53 - 1e-7 <i>i</i>	1.43-1e-8 <i>i</i>	1.43-1e-8 <i>i</i>	1.528-1e-7 <i>i</i>	1.528-1e-7 <i>i</i>	1.43-1e-8 <i>i</i>	1.43-1e-8 <i>i</i>
index	BC: 1.75 - 0.44 <i>i</i> (FF) <sup>d</sup>	1.75-0.44 <i>i</i>	1.85-0.71 <i>i</i>	1.85-0.71 <i>i</i>	1.85-0.71 <i>i</i>	1.75-0.44 <i>i</i>	1.75-0.44 <i>i</i>
550nm	OA: 1.54 - 0.006 <i>i</i> (FF)	1.53-0.006 <i>i</i>	1.53-0.0055 <i>i</i>	1.527-0.014 <i>i</i>	1.527-0.014 <i>i</i>	1.53-0.006 <i>i</i>	1.53-0.006 <i>i</i>
Dust	Dust: 1.52 - 0.0015 <i>i</i>	1.53-0.0055 <i>i</i>	1.517-0.0011 <i>i</i>	1.564-0.002 <i>i</i>	1.564-0.002 <i>i</i>	1.53-0.002 <i>i</i>	1.53-0.008 <i>i</i>
SS	SS: 1.55 - 1e-7 <i>i</i>	1.50-1e-8 <i>i</i>	1.49-1e-8 <i>i</i>	1.45-0. <i>i</i>	1.45-0. <i>i</i>	1.38-4.26e-9 <i>i</i>	1.50- 1e-8 <i>i</i>
	Aged BB: 1.54 - 0.018 <i>i</i>						
Additional Species <sup>f</sup>	NO <sub>3</sub> <sup>-</sup>	-	-	NO <sub>3</sub> <sup>-</sup>	NO <sub>3</sub> <sup>-</sup>	-	-
Dust Size distribution (μm) <sup>g</sup>	6 bins 0.0316-0.1-0.316-1.0-3.16-10-31.6	8 bins 0.1-0.18-0.3-0.6-1.0-1.8-3.0-6.0-10.0	Accum. mode: 0.05< r <sub>m</sub> < 0.5 coarse mode: r <sub>m</sub> > 0.5	5 bins 0.1-1-2-4-8-16	4 bins 0-1-2-4-8	6 bins 0.1-0.22-0.46-1.0-2.15-4.64-10.0	8 bins 0.1-0.18-0.3-0.6-1.0-1.8-3.0-6.0-10.0
References	Bellouin et al., 2011	Chin et al., 2002, 2014	Pozzoli et al., 2011	Tsigaridis et al., 2013	Bauer et al., 2008, 2010	Takemura et al., 2005, 2009	Colarco et al., 2010

352  
353 a Spatial resolutions (°latitude × °longitude × number of vertical levels).

354 b Anthropogenic emission data are from either A2-ACCMIP or A2-MAP (refer to Diehl et al. 2012).

355 c Biomass burning emission data (refer to Diehl et al. 2012).

356 d FF is fossil fuel and BB is biomass burning.

357 e As for EHCAM5-HAMMOZ model with a mixed aerosol scheme, the refractive index for each of the 7 modes is  
358 calculated as the volume weighted average of the refractive indices of the components of the mode, including the  
359 diagnosed aerosol water.360 f Additional aerosols besides commonly included aerosol species, i.e. SO<sub>4</sub><sup>2-</sup> (sulfate), Dust, SS (sea salt), BC (black  
361 carbon), and OA (organic aerosol). Here NO<sub>3</sub><sup>-</sup> is nitrate.362 g Listed is the edges of size bins in all models except for ECH, in which r<sub>m</sub> is modal radii.

371  
372  
373

Table 2. Summary of stations in South Asia used in this study

Type	Station <sup>a</sup>	Lat	Lon	Alt (m)	Popul- ation <sup>b</sup> (milli-)	Data Source <sup>c</sup>	Data Category	Main Feature
Urban	Delhi	28.58° N	77.20° E	260	16.75	ICARB	BC	In western IGP, the largest city in India
	Karachi	24.87° N	67.03° E	49	13	AERONET	AOD	Coastal location in southern Pakistan
	Lahore	31.54° N	74.32° E	270	9	AERONET	AAOD	In western IGP, major agricultural region
	Hyderabad	17.48° N	78.40° E	545	6.81	ICARB	AOD	In central Indian Peninsula
	Pune	18.52° N	73.85° E	559	5.05	ICARB	BC	In western plateau
	Kanpur	26.51° N	80.23° E	123	2.77	AERONET/ISRO-GBP	Misc. <sup>d</sup>	In central IGP
	Agra	27.06° N	78.03° E	169	1.75	ISRO-GBP	Misc. <sup>d</sup>	Between Delhi and Kanpur
Semi-Urban	Allahabad	25.45° N	81.85° E	98	1.22	ISRO-GBP	Misc. <sup>d</sup>	In central-eastern IGP
	Kharagpur	22.52° N	87.52° E	28	0.37	ICARB	BC	In eastern IGP-outflow region to Bay of Bengal
Remote	Hisar	29.09° N	75.42° E	41	0.3	ISRO-GBP	Misc. <sup>d</sup>	Surrounded by agricultural field in western IGP
	Trivandrum	8.55° N	76.90° E	3	0.75	ICARB	BC	A coastal station in southern India
Remote	Port Blair	11.63° N	92.70° E	60	0.1	ICARB	BC	Island in Bay of Bengal
	Nainital	29.20° N	79.30° E	1950	0.04	ICARB	BC	High altitude remote location in the Himalayan foothills
	Minicoy	8.30° N	70.00° E	1	0.009	ICARB	BC	Island in Arabian Sea

374 <sup>a</sup> In decreasing order of the population375 <sup>b</sup> Statistics in 2011 from wikipedia376 <sup>c</sup> Details in section 3.2 and 3.3377 <sup>d</sup> Miscellaneous, including meteorological fields, AOD, AAOD and aerosol surface concentration.378  
379

380  
381

Table 3. The statistics of the aerosol parameters over South Asia (60°E–95°E; 5°N–36°N. Land only) in 2006.

Parameter	Unit	#	Mean	Median	Min	Max	Stdev	Diversity <sup>a</sup>
<b>SO<sub>4</sub></b>								
Emi <sup>b</sup>	Tg(SO <sub>2</sub> ) yr <sup>-1</sup>	7	7.36	7.39	5.81	8.61	0.86	12%
Cheaq <sup>c</sup>	Tg(SO <sub>4</sub> ) yr <sup>-1</sup>	4	0.27	0.28	0.15	0.35	0.10	36%
Cheg <sup>d</sup>	Tg(SO <sub>4</sub> ) yr <sup>-1</sup>	4	0.24	0.18	0.12	0.46	0.16	<b>66% <sup>h</sup></b>
Wet	Tg(SO <sub>4</sub> ) yr <sup>-1</sup>	7	4.38	3.98	3.64	6.21	0.93	21%
Dry	Tg(SO <sub>4</sub> ) yr <sup>-1</sup>	7	0.78	0.77	0.27	1.26	0.35	<b>44%</b>
Dry/Dry+Wet	%	7	19	20	8	29	8	40%
Life time	Days	7	5.02	4.81	3.22	8.50	1.73	34%
Load	Tg(SO <sub>4</sub> )	7	0.06	0.05	0.04	0.08	0.02	26%
MEE <sup>e</sup>	m <sup>2</sup> g <sup>-1</sup> (SO <sub>4</sub> )	4	8.56	8.99	5.58	10.68	2.15	25%
AOD	Unitless	4	0.07	0.07	0.04	0.08	0.02	27%
<b>BC</b>								
Emi	Tg yr <sup>-1</sup>	7	0.70	0.71	0.59	0.78	0.06	9%
Wet	Tg yr <sup>-1</sup>	7	0.27	0.28	0.21	0.31	0.04	15%
Dry	Tg yr <sup>-1</sup>	7	0.15	0.19	0.05	0.21	0.07	46%
Dry/Dry+Wet	%	7	33	37	15	41	10	29%
Life time	Days	7	7.67	6.56	4.13	15.82	3.84	<b>50%</b>
Load	Tg	7	0.008	0.007	0.005	0.014	0.003	39%
MEE	m <sup>2</sup> g <sup>-1</sup>	4	7.07	7.56	2.77	10.40	3.63	<b>51%</b>
AOD	Unitless	4	0.008	0.010	0.003	0.011	0.004	45%
<b>OA</b>								
Emif <sup>f</sup>	Tg yr <sup>-1</sup>	7	3.69	3.58	2.77	4.46	0.61	16%
Wet	Tg yr <sup>-1</sup>	7	1.68	1.62	1.26	2.31	0.37	22%
Dry	Tg yr <sup>-1</sup>	7	0.78	0.82	0.31	1.21	0.32	<b>41%</b>
Dry/Dry+Wet	%	7	35	38	20	44	10	<b>29%</b>
Life time	Days	7	5.60	5.25	4.44	7.09	1.07	19%
Load	Tg	7	0.05	0.04	0.03	0.07	0.01	25%
MEE	m <sup>2</sup> g <sup>-1</sup>	4	5.17	4.99	3.69	7.00	1.39	27%
AOD	Unitless	4	0.023	0.022	0.018	0.030	0.005	21%
<b>DUST</b>								
Emi	Tg yr <sup>-1</sup>	7	103.84	43.34	6.43	367.28	128.23	<b>124%</b>
Wet	Tg yr <sup>-1</sup>	7	43.43	41.07	11.82	92.55	24.47	56%
Dry + Sed <sup>g</sup>	Tg yr <sup>-1</sup>	7	98.50	46.92	1.34	316.87	113.42	<b>115%</b>
Dry/Dry+Wet	%	7	56	68	12	84	26	47%
Life time	Days	7	3.86	4.17	1.08	6.92	1.98	51%
Load	Tg	7	0.87	0.91	0.16	1.43	0.39	45%
MEE	m <sup>2</sup> g <sup>-1</sup>	4	0.64	0.59	0.50	0.89	0.17	27%
AOD	Unitless	4	0.10	0.09	0.08	0.12	0.02	22%
<b>TOTAL</b>								
AOD	Unitless	7	0.21	0.18	0.16	0.33	0.06	28%
AAOD	Unitless	7	0.02	0.02	0.01	0.02	0.01	37%

382

383 a. The diversity is defined as the ratio of standard deviation and mean (i.e. stdev/mean). The largest and second  
384 largest diversities in each species are highlighted in bold.385 b. The emission of SO<sub>2</sub>, including anthropogenic and biomass burning emission.386 c. The chemical production of SO<sub>4</sub> in aqueous phase reaction (i.e. SO<sub>2</sub> reacts with H<sub>2</sub>O<sub>2</sub>).387 d. The chemical production of SO<sub>4</sub> in gaseous phase reaction (i.e. SO<sub>2</sub> reacts with OH).

388 e. Mass extinction efficiency, defined as the ratio of AOD and load (i.e. AOD/load).

389 f. Sum of anthropogenic emission, biomass burning emissions and secondary organic aerosol.

390 g. Dry deposition plus sedimentation.

391 h. The top two largest diversities in each species are highlighted in bold.

392

393 **Figures**

## 394 Captions

395

396 Fig. 1. Topography of South Asia and the locations of the stations used in this study. Three  
397 AERONET stations are labeled in blue, eight ICARB stations in red, and four ISRO-GBP stations in  
398 black except for Kanpur. The topography map is obtained from  
399 <http://mapofasia.blogspot.com/2013/02/map-of-south-asia-area-pictures.html>.

400

401 Fig. 2. Spatial distribution of anthropogenic emissions of BC, OC, SO<sub>2</sub>, NH<sub>3</sub> and NO<sub>x</sub> averaged for  
402 2000-2007 from A2-ACCMIP emission dataset (units: g m<sup>-2</sup> yr<sup>-1</sup>) over South Asia (60°E–95°E; 5°N  
403 –36°N). The annual mean emission amount over South Asia (land only) is shown at the bottom.

404

405 Fig. 3. Spatial distribution of biomass burning emission of BC based on GFED2 for each season  
406 averaged for 2000-2007 (units: g C m<sup>-2</sup> yr<sup>-1</sup>) over South Asia (60°E–95°E; 5°N –36°N). The  
407 seasonal mean emission amount over South Asia (land only) is shown at the bottom. Note that the  
408 color scale is the same as that of BC in the Fig. 2 for the purpose of comparison.

409

410 Fig. 4. The annual averaged mean AOD for 2000-2007 over region: (a) South Asia (60°E–95°E; 5°N  
411 –36°N, averaged over land only, i.e. the gray area in the map); (b) Central IGP (77°E-83°E; 25°N–  
412 28°N, averaged over the red box on the map shown in Fig. 4a). Thin lines with symbols represent  
413 seven models, and thick lines represent four satellite datasets. Multi-year averaged mean AOD and  
414 the standard deviation is listed on each panel.

415

416 Fig. 5. Monthly mean AOD (left column) and AAOD (right column) at three AERONET stations in  
417 South Asia. The gray bar represents data from AERONET, the thin lines represent results from  
418 seven models, and symbols represent the data from three satellite retrievals. On each panel, corr is  
419 correlation coefficient of a model with AERONET, bias is relative mean bias, i.e.  $\Sigma$   
420  $(AOD_{MODEL_i})/\Sigma (AOD_{AERONET_i})$ , and rmse is root-mean-square error relative to AERONET.

421

422 Fig. 6. Monthly AOD of total aerosol (aer) and components (ss, so<sub>4</sub>, bc, oa, dust, no<sub>3</sub>, soa and bb) at  
423 Kanpur in 2004 from four models, HAD (upper left), GOC (upper right), GE5 (lower left), and SPR  
424 (lower right). The gray bar represents total AOD from AERONET, and the lines represent the  
425 model results of total AOD (black line) and component AODs (colored lines). The corresponding  
426 annual mean values are also listed. NOTE: For the HAD model, bc and oa are only from fossil fuel  
427 sources; the biomass burning aerosol is labeled "bb".

428

429 Fig. 7a. Spatial distribution of AOD over South Asia in four seasons averaged for 2000–2007 from  
430 four satellite datasets (MODIS-Terra, MODIS-Aqua, MISR, and SeaWiFS). The corresponding area  
431 averaged seasonal mean AOD value over land is listed on each panel. Three AERONET stations  
432 used in this study are labeled in the maps for references. Area in white means no retrieval  
433 available due to the presence of bright surface or frequent cloud cover.

434

435 Fig. 7b. Spatial distribution of AOD over South Asia in four seasons averaged for 2000–2007 from  
436 seven models (the first three models using the anthropogenic emissions from A2-MAP and the rest  
437 using A2-ACCMIP). The area averaged seasonal mean AOD value over land is listed on each panel.  
438 Three AERONET stations used in this study are shown on the maps for references.

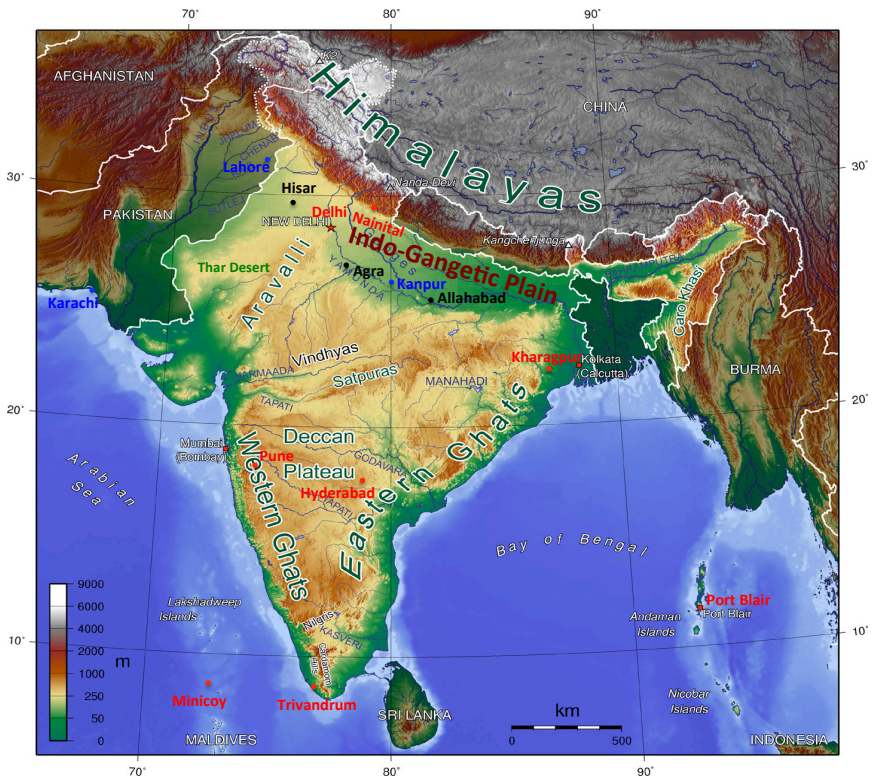
440 Fig. 8. Seasonal mean of vertical profile of extinction coefficient (units:  $\text{km}^{-1}$ ) at (a) Kanpur, and (b)  
441 Hyderabad from CALIOP and seven models. The corresponding seasonal mean AOD, Za (units: km)  
442 and  $F_{2\text{km}}$  are listed after each symbol name. The gray shaded area in CALIOP is one standard  
443 deviation relative to the average of 2006-2011.

444  
445 Fig. 9. Monthly mean surface BC concentration at eight ICARB stations in 2006 (units:  $\mu\text{g m}^{-3}$ ).  
446 Gray bar represents measurement from ICARB and thin lines represent seven models.

447  
448 Fig. 10. Comparisons of seven models against ISRO-GBP campaign measurements at four IGP  
449 stations (Hisar, Agra, Kanpur, Allahabad from western to eastern IGP) in December 2004. The  
450 variables include meteorological fields of surface relative humidity (1st row) and surface  
451 temperature (2nd row), aerosol species mass concentrations of  $\text{SO}_4^{2-}$  (3rd row),  $\text{NO}_3^-$  (4th row),  
452 BC (5th row), and OA (6th row), and columnar AOD (7th row) and AAOD (8th row) at 550nm.  
453

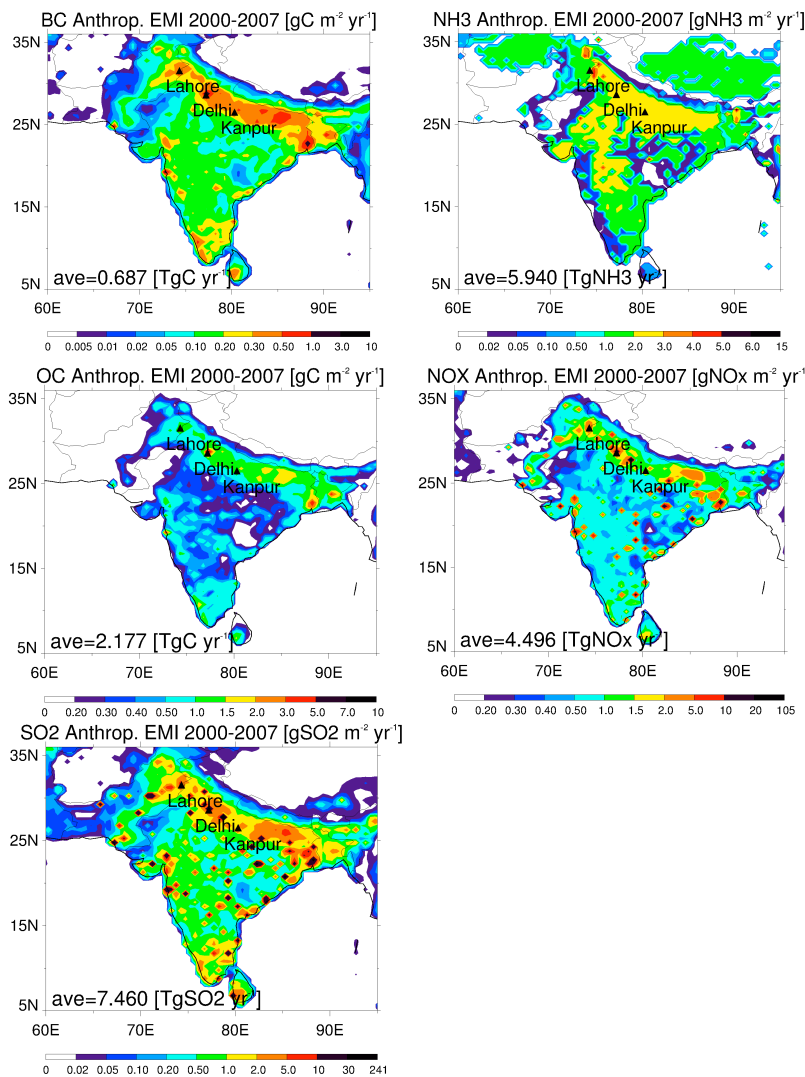
454 Fig. 11. Mass extinction efficiency (MEE) at 550nm for individual aerosol components (units:  $\text{m}^2 \text{ g}^{-1}$ )  
455 as a function of relative humidity (RH). For  $\text{SO}_4^{2-}$ , OC and BC, MEE is calculated using the  
456 relationship of RH and size growth based on optical properties of aerosols and clouds (OPAC)  
457 (Hess et al., 1998). For  $\text{NO}_3^-$ , MEE is calculated according to the work by A. Lacis  
458 ([http://gacp.giss.nasa.gov/data\\_sets/lacis/introduction.pdf](http://gacp.giss.nasa.gov/data_sets/lacis/introduction.pdf)).

459  
460  
461  
462  
463  
464  
465  
466



467  
468 Fig. 1.

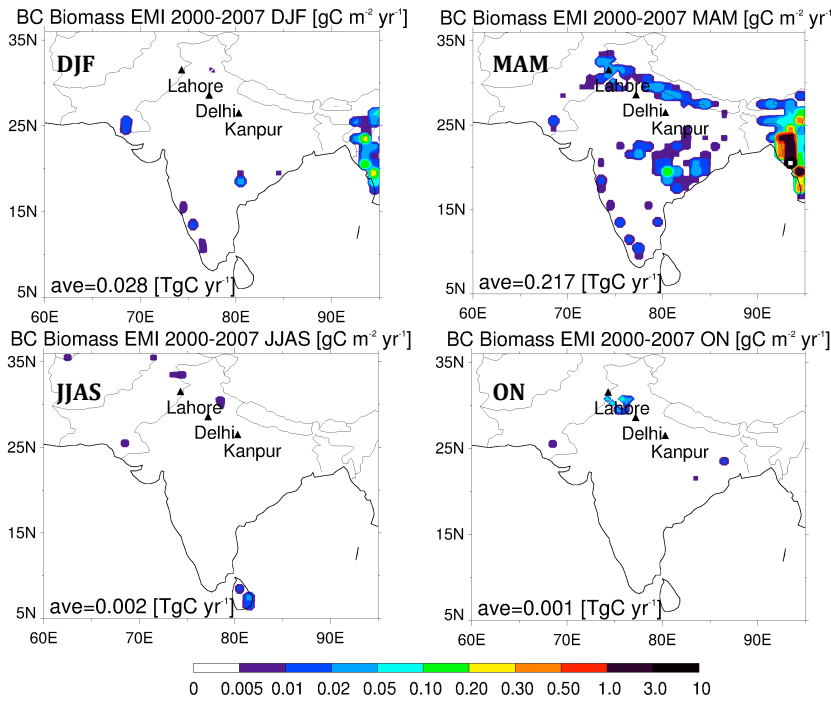
469



470

471 Fig. 2.

472



473

474

475 Fig. 3.

476

477

478

479

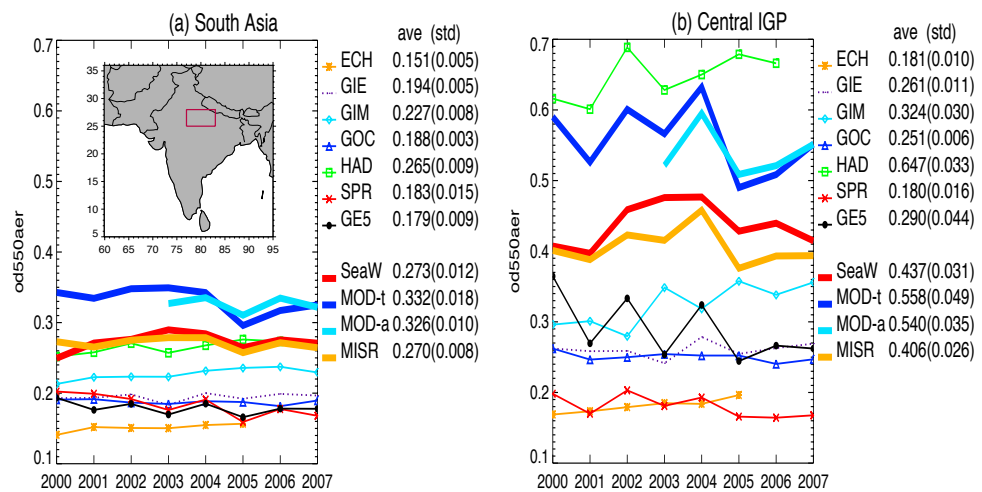
480

481

482

483

Annual mean AOD (2000-2007)



485 Fig. 4.

486

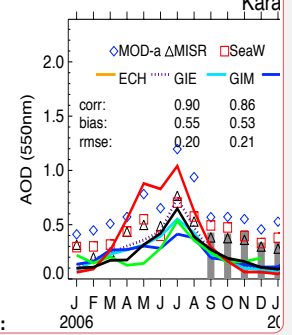
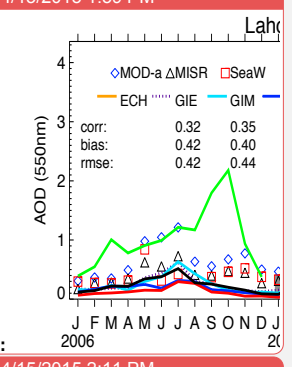
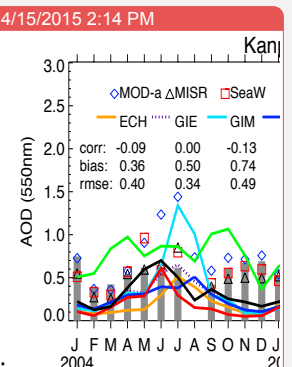
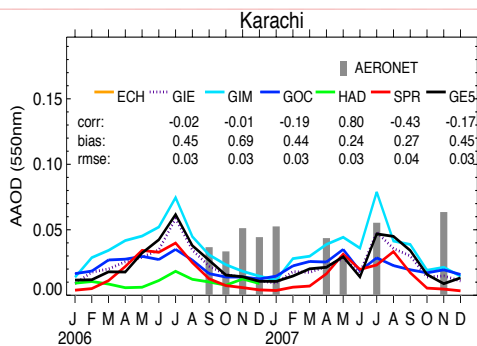
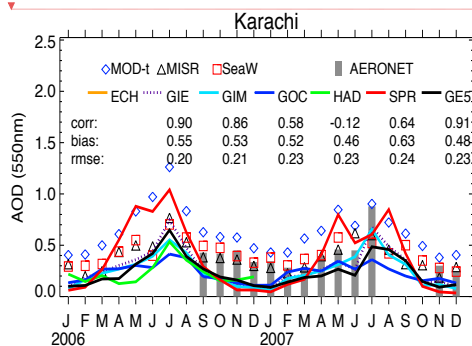
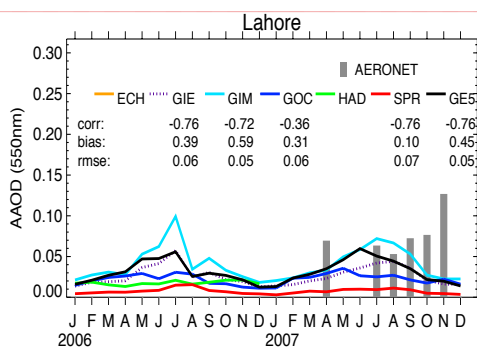
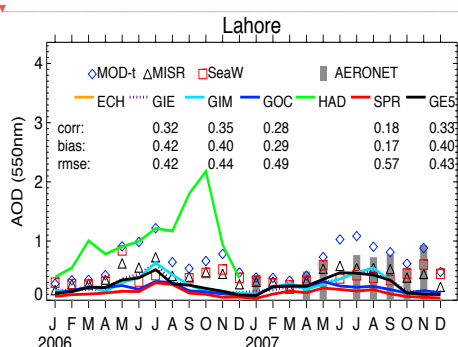
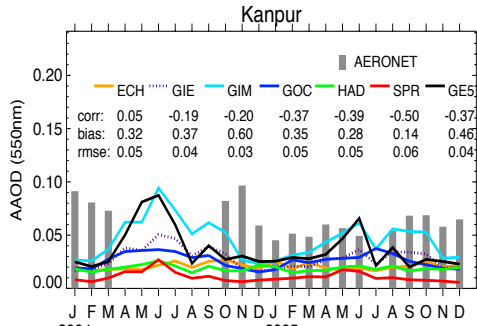
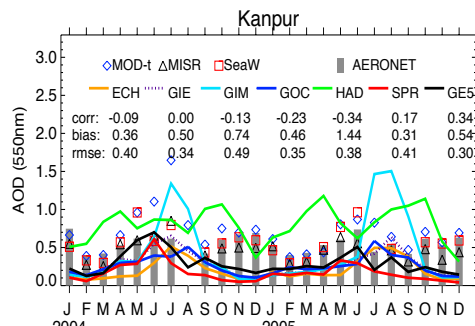
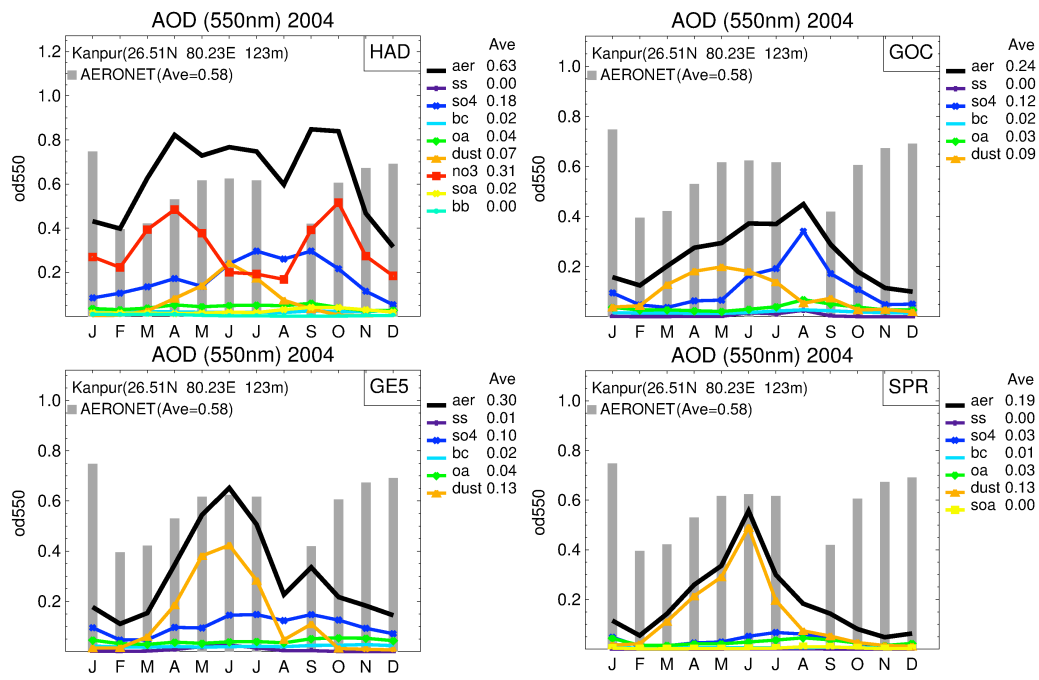


Fig. 5.

494

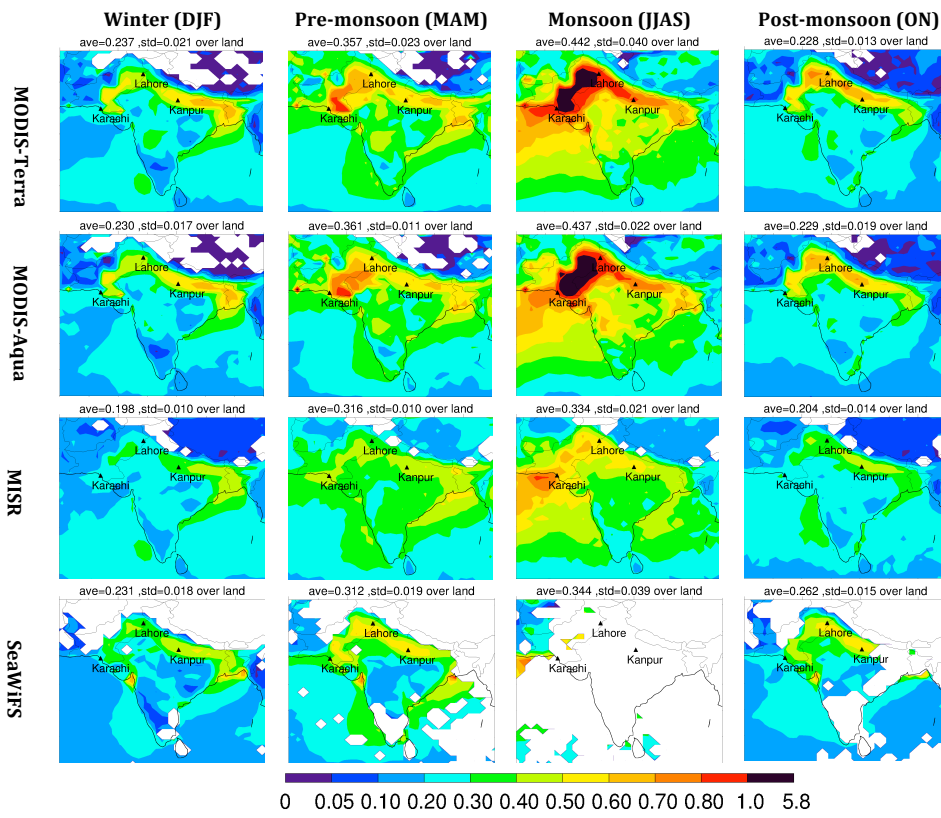


495

496 Fig. 6.

497

498



500 Fig. 7a

501  
502  
503  
504  
505  
506  
507  
508  
509  
510  
511  
512  
513  
514  
515  
516

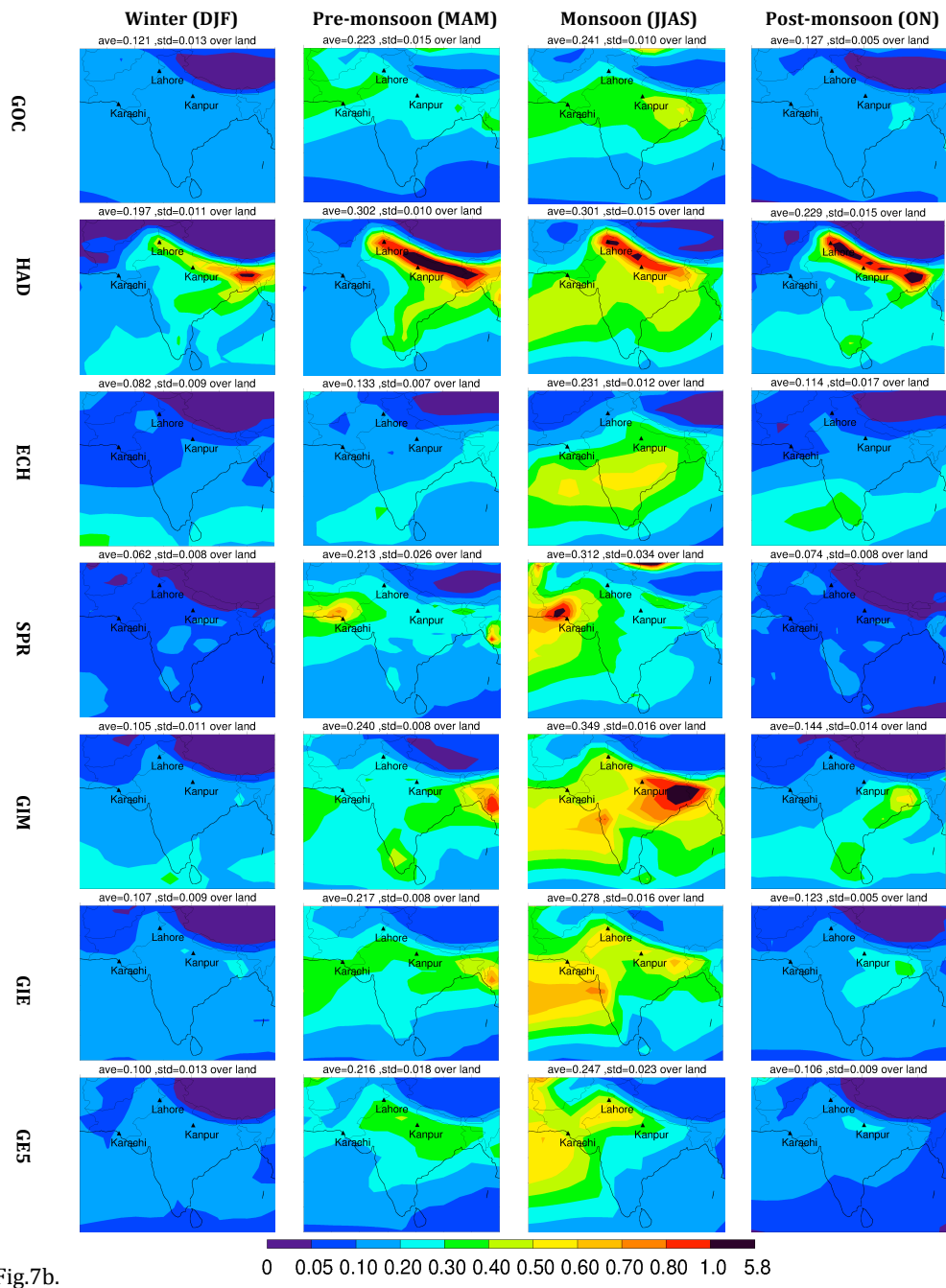
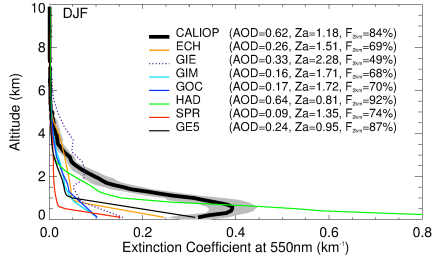
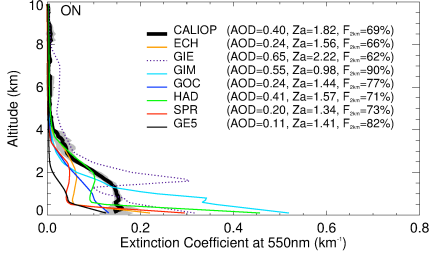
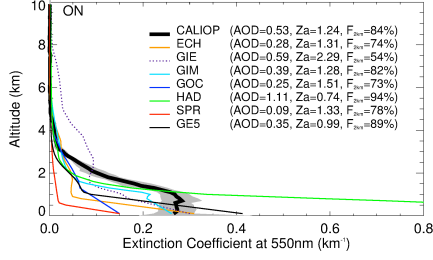
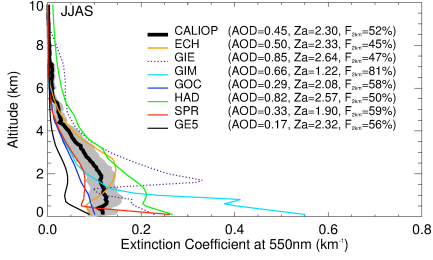
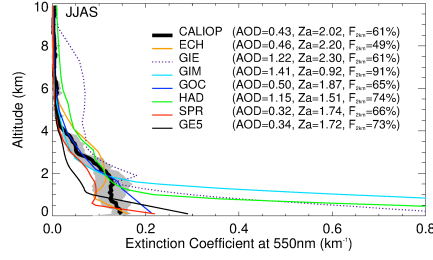
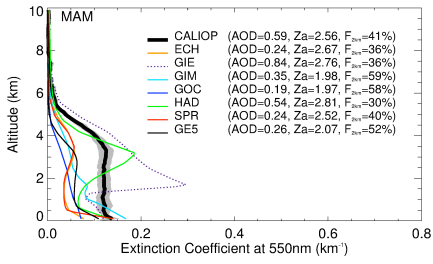
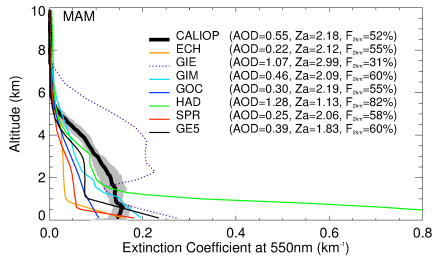
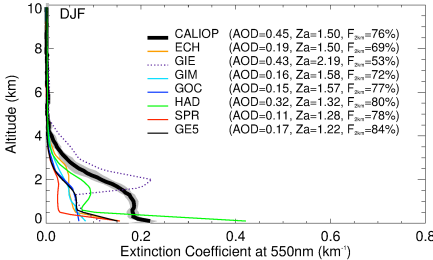


Fig.7b.

(a) Kanpur



(b) Hyderabad



### Surface BC concentration for 2006

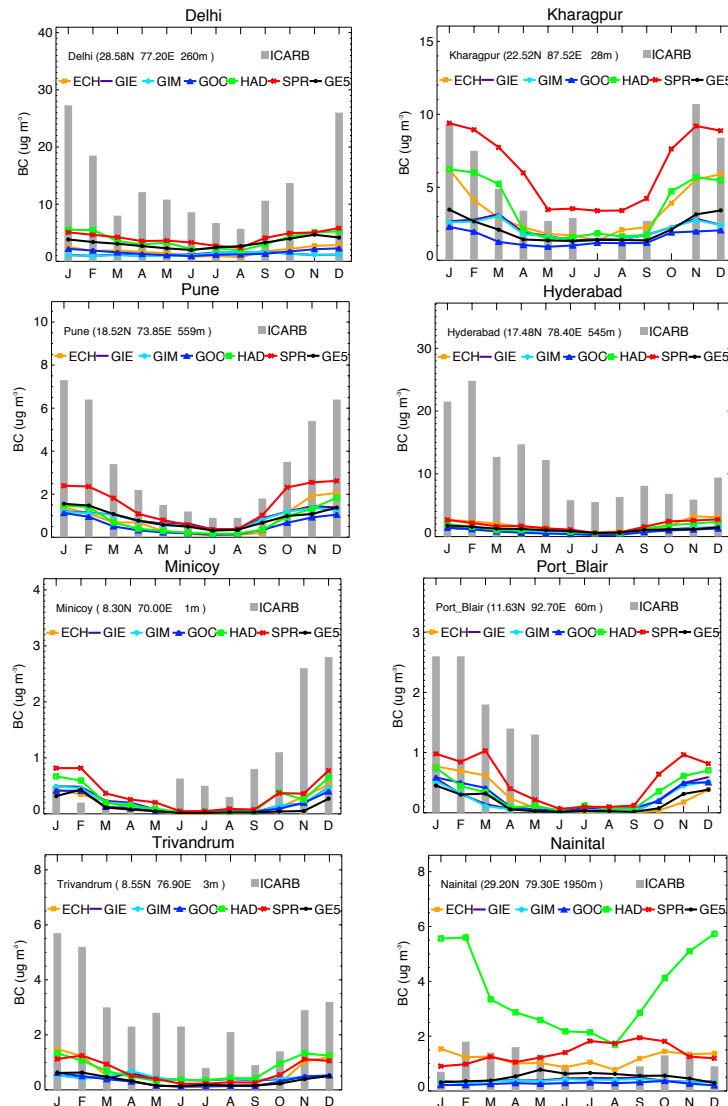
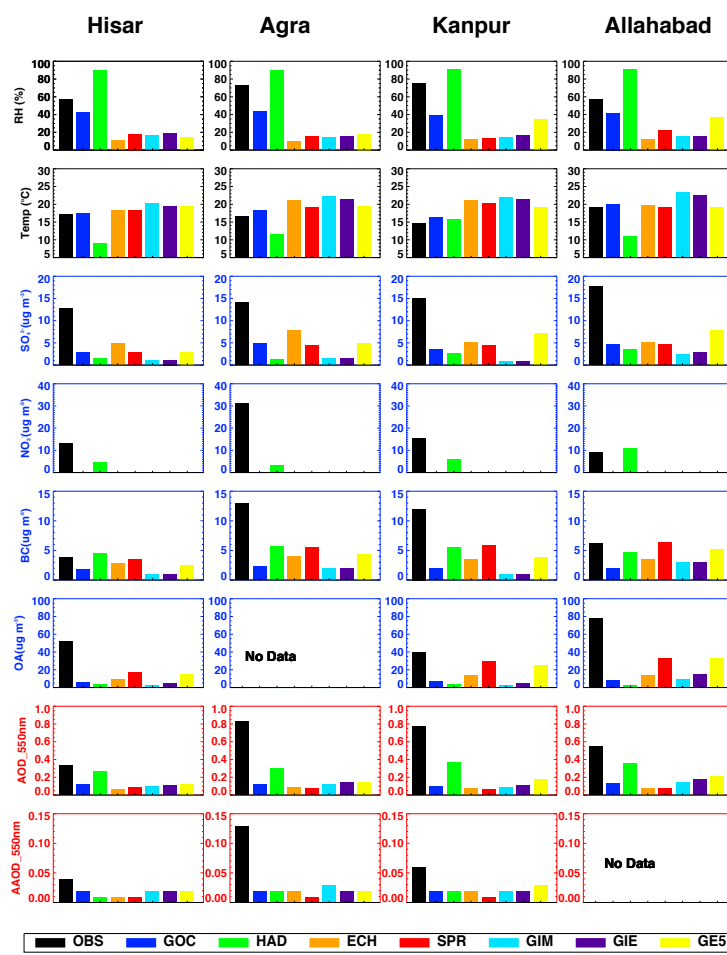


Fig. 9.

523



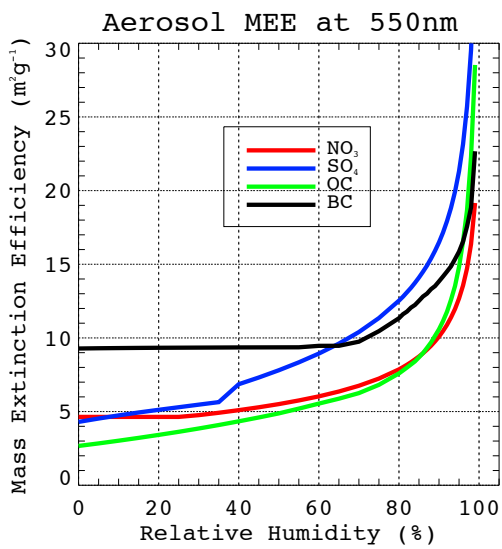
524

525

526

527 Fig.10.

528



529  
530  
531 Fig. 11.  
532  
533  
534  
535